Zener tunneling and localization in small conducting rings

Gianni Blatter*
Laboratory for Atomic and Solid State Physics, Cornell University, Clark Hall, Ithaca, New York 14853-2501 and Brown Boveri Research Center, CH-5405 Baden, Switzerland

Dana A. Browne†
Laboratory for Atomic and Solid State Physics, Cornell University, Clark Hall, Ithaca, New York 14853-2501
(Received 10 August 1987)

We study the single-particle properties of an electron in a small one-dimensional conducting ring subject to a large uniform electric field which is generated by a linearly ramped magnetic flux. The adiabatic eigenstates of this system form a complete set of minibands which are separated by gaps determined by the static scattering potential in the ring. At high fields the Zener tunneling transitions between these minibands promote the particles to higher energy states. In spite of the absence of inelastic scattering in this model, D. Lenstra and W. van Haeringen [Phys. Rev. Lett. **57**, 1623 (1986)] found a resistive behavior of the electrons which they attributed to the process of phase randomization generated by Zener tunneling between the minibands. We have studied several model systems to investigate the roles of phase randomization and of the energy dependence of the Zener tunneling amplitudes. None of the models studied showed resistive behavior. We find that the process of phase randomization alone (constant Zener tunneling amplitudes) leads to an exponential localization of the electrons in energy space. The addition of energy-dependent Zener tunneling amplitudes weakens the localization. Our main conclusion is that the process of phase randomization leads to localization of the electrons in energy space and not to resistive behavior.

I. INTRODUCTION

As the dimensions of a sample become smaller than the distance between inelastic scattering events, a new "mesoscopic" regime is reached where the transport properties are strongly affected by quantum-mechanical interference.[1] The maintenance of the quantum coherence of the single-particle waves throughout the sample leads to sample-specific conductance and to reproducible variations in the transport coefficients as the chemical potential or the magnetic field is changed. Outstanding experimental achievements include the observations of (universal) conductance fluctuations in thin wires[2,3] and of periodic structure in the magnetoresistance of small (semi)conducting rings[4,5] (Aharanov-Bohm effect).

An elementary example which has been studied thoroughly both experimentally[4] and theoretically[1,6-9] is the normal metal ring threaded by a magnetic flux Φ. Let us consider a one-dimensional closed loop. Because of the periodic boundary conditions enforced by the single valuedness of the wave functions, the eigenstates of the electrons in this system look like Bloch waves in a crystal.[6,8] In the transcription, the circumference L of the ring corresponds to the lattice constant a in the crystal. The role of the wave vector k in the crystal is taken up by the flux parameter $\alpha/L=2\pi\Phi(t)/\Phi_0 L$, where $\Phi_0=hc/e$ is the normal state flux quantum in Gaussian units. As we increase the flux $\Phi(t)$ through the loop linearly in time, a constant electric field F is induced in the ring. The flux parameter α then increases linearly in time, corresponding to a Bloch electron moving linearly in time through k space.

The effect of a nonuniform potential in the ring is to introduce "minigaps" at the zone boundaries $\alpha=\pm n\pi$ which are reached by the electron whenever the flux $\Phi(t)$ goes through a multiple of half the flux quantum, $\Phi_0/2$. Since the spectrum of the system is discrete, an electron in a pure Bloch state will follow the flux change adiabatically if the induced electric field is infinitesimal, i.e., it will be backscattered to the same energy level each time it reaches a zone boundary. If the field strength is increased, the possibility of Zener tunneling[10] between the energy levels arises, i.e., the electron can be forward scattered to the neighboring level as it crosses a zone boundary.

Whereas the properties of normal metal rings in the adiabatic limit of weak electric fields are reasonably well understood, the situation for high electric fields is much less clear. A recent paper by Lenstra and van Haeringen[11] suggested that very interesting phenomena are present in the high-field limit. Applying their theory of the dc conductivity of a one-dimensional (1D) wire with periodic boundary conditions[12-14] to the closed loop they found a "resistive" behavior in this Hamiltonian system: the average steady current turned out to be proportional to the electric field in the ring induced by the time-dependent flux $\Phi(t)$. This behavior is quite unusual—the fundamental microscopic Zener tunneling amplitudes,[10] which produce this current, are not analytic in the electric field, yet the macroscopic result, Lenstra and van Haeringen claimed, *is* linear in the field. In their paper they attributed this resistive behavior to the occurrence of phase randomization induced by Zener tunneling between the discrete energy levels of the system.

The claim of a resistive behavior in a Hamiltonian system has been criticized by Landauer[15,16] who showed that the process of Zener tunneling is in fact completely reversible,[17] and thus concluded that the system was acting more like a nonlinear inductance than a resistance, so that stored energy could in principle be retrieved. This was in fact seen in the numerical simulations by Lenstra and van Haeringen.[11,18]

The time evolution of the single-particle wave function in the ring can be cast in the form of a scattering problem. After this reformulation, the time evolution of the system depends on two sets of parameters, (i) the amplitudes t_n for Zener tunneling between the bands, and (ii) the phases Θ_n for free propagation between two successive scattering events (here n numbers the adiabatic energy levels).

The purpose of the present paper is to investigate the origin of the apparently "Ohmic" or resistive behavior of the system reported by Lenstra and van Haeringen. To do so we have studied four models: (i) Their suggestion that phase randomization might be responsible for the saturating current lead us to isolate this property and to first study a model with constant Zener tunneling amplitudes $t_n = t$ but quasirandom phases Θ_n. (ii) We repeated the simulations on the Kronig-Penney model over a much longer time scale, as we found that the system does not reach its asymptotic behavior on the short time scale considered by Lenstra and van Haeringen. (iii) We have studied a system which is characterized by a realistic set of gaps which close at high energies (screened impurity model), unlike the Kronig-Penney model where the gaps asymptotically approach a constant value. (iv) We have studied a model characterized by periodic phases Θ_n and constant Zener tunneling amplitudes $t_n = t$. Models (i) to (iii) are studied mainly by numerical methods and the discussion of model (iv) includes both analytical and numerical work.

This extensive study of the system leads us to the following conclusions: (i) For constant Zener tunneling amplitudes the phase randomization in this system leads to exponential localization of the wave function in energy space (i.e., the probability to find an electron in a high energy state decays exponentially with increasing energy) and a zero-mean-current asymptotic state. (ii) Relaxing the phase randomization by introducing periodic phases $\Theta_n = \Theta_{n+p}$ changes the nature of the wave function from localized to extended. The current then rises linearly in time, indicating free-electron-like acceleration. (iii) As we relax the condition of constant Zener tunneling amplitudes we find results indicating that the wave functions are algebraically localized for the Kronig-Penney model. Accordingly, the current again returns back to a zero mean for all field values; however, the time needed to reach the asymptotic state is much longer. We wish to point out that these results for the Kronig-Penney model are somewhat speculative and further studies have to confirm or reject them. However, we definitely do not observe Ohmic behavior: whereas we can reproduce Lenstra and van Haeringen's results on a short time scale, we find that the apparent saturation of the current is only a transient effect and *not* the asymptotic behavior of the system.

It turns out that the Kronig-Penney model can be regarded as an intermediate case between models showing either localized or delocalized wave functions. (iv) For the screened impurity model we then find that the wave functions are delocalized. However, also in this model the phase randomization is very important since it can prevent the particles from rapidly attaining large energies in the electric field. At not too high fields and for finite times the system behaves as if the particles were actually localized.

The outline of the paper is as follows. In Sec. II we describe briefly the low-field (adiabatic) and high-field behavior of electrons in a one-dimensional closed loop. We introduce Zener tunneling and show how to reduce the time evolution to a scattering problem. We also introduce the notion of quasienergy. In Sec. III we present our results for the three models characterized by constant Zener tunneling amplitudes and quasirandom phases, the Kronig-Penney model, and the screened impurity model. The results of this section are found by numerical simulations. In Sec. IV we first analytically study the simplest cases of a system with periodic phases $\Theta_n = \Theta_{n+2}$ and $\Theta_n = \Theta_{n+4}$. We then present numerical results on systems with larger periods: This allows us to turn on the phase randomization gradually and clarifies how the localization of the wave functions occurs in this system. In Sec. V we summarize our results and conclude. In order to make this paper self-contained we include an Appendix A in which we derive the adiabatic energy levels and eigenstates for the Kronig-Penney model in a simple way, and an Appendix B discussing Zener tunneling.

II. ELECTRONS IN A RING

We will start by briefly reviewing the physics of an isolated 1D ring threaded by a magnetic flux $\Phi(t) = cFLt$ which is ramped linearly in time (c is the velocity of light, $F > 0$ is the induced electric field in the ring whose circumference is L). It is important that this is a Hamiltonian system and therefore unable to dissipate energy. We shall start with the adiabatic limit, which applies to a slowly varying flux, and then generalize the formalism to describe fields of arbitrary strength. As we integrate the time evolution of the system over the time period $t_\pi = \pi\hbar/eFL$, half the period of Bloch oscillations ($e > 0$ is the electron charge), the formalism reduces to a scattering problem between the adiabatic energy levels with the scattering amplitudes determined by Zener tunneling and backscattering.[12] Thereby, the time evolution of the system is reduced to a discrete set of points and can be described by the iterative application of a unitary operator T. In a third subsection we will introduce the quasienergy and the corresponding eigenfunctions which diagonalize the discrete time evolution operator T.

We consider a 1D ring with the time varying magnetic flux threading it. Since we are interested in the problem of a spacially constant and time-independent electromotive force (emf) we will take a choice of gauge where the scalar potential is zero and the vector potential

$A(t)=cFt$ is linear in time. The Hamiltonian is then given by

$$H(t)=\frac{1}{2m}\left[\frac{\hbar}{i}\frac{\partial}{\partial x}+\frac{e}{c}A(t)\right]^2+V(x)\ , \tag{1}$$

where m is the mass of the electron. The potential $V(x)$ is periodic in the circumference L of the ring, $V(x)=V(x+L)$, and describes some scattering potential acting on the electrons. Furthermore, the Hamiltonian (1) shows the time reversal symmetry $H(-t)=H^*(t)$.

The wave functions $\Psi(t)$, describing the single-particle states of the system, satisfy the Schrödinger equation

$$i\hbar\frac{\partial\Psi(t)}{\partial t}=H(t)\Psi(t)\ ,$$

and are subject to periodic boundary conditions, $\Psi(x+L,t)=\Psi(x,t)$, since they must be single-valued functions over the ring.

A. Adiabatic limit

In the adiabatic limit of a slowly varying flux $\Phi(t)$, such that $F\to 0$, we can treat the vector potential $A(t)$ in (1) as a constant parameter. The adiabatic eigenfunctions $u_{n,\alpha}$ and energies $\varepsilon_{n,\alpha}$ then satisfy the time-independent Schrödinger equation

$$H(\alpha)u_{n,\alpha}=\varepsilon_{n,\alpha}u_{n,\alpha}\ , \tag{2}$$

and are subject to the boundary condition $u_{n,\alpha}(x+L)=u_{n,\alpha}(x)$. Here we have introduced the new time (or flux) variable

$$\alpha=2\pi\Phi(t)/\Phi_0=eFLt/\hbar\ ,$$

with $\Phi_0=hc/e$ the unit of flux. In the following we will use the parameters t or α to describe the time coordinate at our convenience.

By removing the vector potential in (2) with a gauge transformation

$$u_{n,\alpha}=e^{-i\alpha x/L}\varphi_{n,\alpha}\ , \tag{3}$$

the problem reduces to calculating the Bloch functions $\varphi_{n,\alpha}$ in a periodic potential $V(x)$,

$$H(0)\varphi_{n,\alpha}=\varepsilon_{n,\alpha}\varphi_{n,\alpha}\ , \tag{4a}$$

$$\varphi_{n,\alpha}(x+L)=e^{i\alpha}\varphi_{n,\alpha}(x)\ , \tag{4b}$$

where $\alpha/L=eFt/\hbar$ is analogous to the wave vector in the usual formulation of the Bloch problem and the "lattice constant" is given by the ring's circumference L. The wave functions $\varphi_{n,\alpha}(x)$ and eigenenergies $\varepsilon_{n,\alpha}$ are calculated exactly in Appendix A for the case of a δ-function scattering potential $V(x)=V_0\delta(x)$—the Kronig-Penney model. A plot of the adiabatic energy levels $\varepsilon_{n,\alpha}$ is shown in Fig. 1. Both the eigenfunctions $\varphi_{n,\alpha}$ and the eigenenergies $\varepsilon_{n,\alpha}$ are periodic in the flux $\Phi(t)$ with period Φ_0 (Ref. 19) (in α the period is 2π) as is obvious from (4) and illustrated in Fig. 1. The Brillouin zone for the ring is given by the range $[-\pi,\pi]$ of α. Since the unit cell length L in this problem is identical to the Born–von Kármán unit cell, each level contains at most one electron (per spin). The gaps between the minibands $\varepsilon_{n,\alpha}$ are caused by the potential $V(x)$. For the Kronig-Penney model the gap parameter $2\Delta_n$ approaches an asymptotic value $2V_0/L$ as the level index n becomes large. This is identical to the result found by Lenstra and van Haeringen using degenerate perturbation theory. Using a smooth potential instead, leads to gaps which vanish as the energy increases. This is readily understood by noticing that at large energies the perturbative approach is always valid and therefore the gap parameter Δ_n is simply given by the nearly-free-electron approximation

$$\Delta_n=\left|\frac{1}{L}\int_{-L}^{0}dx\ V(x)e^{-i2\pi nx/L}\right|\ .$$

Here the factor $2\pi n/L$ in the exponent is simply the difference in the wave vectors $K_n=\pm n\pi/L$ at opposite sides of the nth Brillouin zone.

The current carried by a single electron in the state $\Psi(t)$ is given by

$$j(t)=\frac{e}{L}\int_{-L}^{0}dx\frac{\hbar}{2mi}\left[\left(\Psi^*\frac{\partial\Psi}{\partial x}-\Psi\frac{\partial\Psi^*}{\partial x}\right)-\frac{2ie}{\hbar c}A\Psi^*\Psi\right]\ , \tag{5}$$

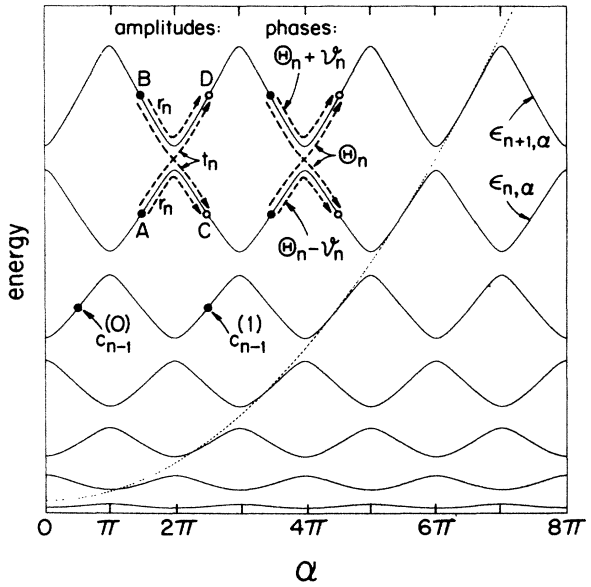

FIG. 1. Adiabatic energy levels $\varepsilon_{n,\alpha}$ as a function of flux α. For a linearly increasing flux the electrons move through the minibands, changing to neighboring minibands by forward scattering (Zener tunneling, $A\to D$ or $B\to C$) or remaining in the same miniband upon back scattering ($A\to C$ or $B\to D$). The transition amplitudes for forward scattering (Zener tunneling) and backscattering are t_n and r_n, respectively. The phase change over one complete scattering event is Θ_n for forward scattering into the $n+1$st level and $\Theta_n-\vartheta_n$ for backscattering into the nth level. The time evolution is calculated by iterating the amplitudes $c_n^{(k)}$ forward in time, where k denotes the kth time step. Also shown is the free-electron parabola for a carrier moving in a uniform potential V_0/L (dotted line).

which for a particle in the pure adiabatic state $u_{n,\alpha}$ reduces to

$$j(t)=\frac{e}{\hbar}\frac{d\varepsilon_{n,\alpha}}{d\alpha} .$$

In the adiabatic limit the particle moves through the miniband in accordance with the flux change $\alpha\Phi_0/2\pi$. As pointed out by Büttiker, Imry, and Landauer[6] this leads to a Josephson-like oscillating current as the particle is Bragg reflected each time it approaches the neighboring level at the Brillouin-zone boundaries. If the flux is fixed at a value differing from an integer multiple of half the unit flux, a constant Josephson-like current is induced in the ring.

As we drop the approximation of infinitely slowly varying flux the possibility of Zener tunneling between the adiabatic levels $u_{n,\alpha}$ leads to new interesting phenomena.

B. Zener tunneling

A strong electric field F along the ring induces transitions between the levels $\varepsilon_{n,\alpha}$. Such nonadiabatic transitions were first studied by Zener[10] and later considered by Eilenberger[20] in the context of interband tunneling in a large electric field in semiconductors. The formulas presented in this section are derived in Appendix B for the Kronig-Penney model.

As Zener tunneling between the single-particle levels becomes important the wave function $\Psi(t)$ spreads over all the adiabatic eigenstates $u_{n,\alpha}$ and therefore is a superposition

$$\Psi(t)=\sum_{n=1}^{\infty} c_n(t)u_{n,\alpha} .$$

The time evolution of the coefficients $c_n(t)$ is determined by the time-dependent Schrödinger equation (1),

$$i\frac{dc_n(\alpha)}{d\alpha}=\frac{\varepsilon_{n,\alpha}}{eFL}c_n(\alpha)-i\sum_{m=1}^{\infty} A_{nm}(\alpha)c_m(\alpha) , \tag{6a}$$

with

$$A_{nm}(\alpha)=\int_{-L}^{0} dx\, u^{*}_{n,\alpha}(x)\frac{du_{m,\alpha}(x)}{d\alpha} . \tag{6b}$$

It turns out that transitions are most probable between neighboring levels as they approach each other at the edge of a Brillouin zone. For example, the coupling between the levels n and $n+1$ in Fig. 1 is strongest for $\alpha=2l\pi$, the coupling between $n-1$ and n for values $\alpha=(2l+1)\pi$.

If we restrict the dynamics to discrete points $\alpha_l=\pi(l+\frac{1}{2})$, $l=0,1,\ldots$, we can reformulate the problem of the time evolution as a scattering problem. We integrate the time evolution (6a) over the interval spanned by α_l and α_{l+1}, taking into account only transitions between neighboring (approaching) levels. The unitary matrix S_n then describes the time evolution of the pair of amplitudes c_n and c_{n+1} over the time interval t_π:

$$\begin{bmatrix} c_{n+1}(\alpha_{l+1}) \\ c_n(\alpha_{l+1}) \end{bmatrix}=S_n \begin{bmatrix} c_{n+1}(\alpha_l) \\ c_n(\alpha_l) \end{bmatrix}$$
$$=e^{-i\Theta_n}\begin{bmatrix} r_n e^{-i\vartheta_n} & it_n \\ it_n & r_n e^{i\vartheta_n} \end{bmatrix}\begin{bmatrix} c_{n+1}(\alpha_l) \\ c_n(\alpha_l) \end{bmatrix} . \tag{7}$$

The amplitudes $c_{n+1}(\alpha_l)$, $c_n(\alpha_l)$ and $c_{n+1}(\alpha_{l+1})$, $c_n(\alpha_{l+1})$ correspond to the incoming and outgoing states in the usual scattering formalism, respectively. Assuming that the transition is completed (i.e., points A, B, and C, D in Fig. 1 are in the asymptotic regions of the scattering event) the amplitudes for Zener tunneling t_n (transition from A to D in Fig. 1) and backscattering r_n (transition from A to C) are given by

$$t_n=\exp\left[-\frac{\pi^2}{4}\frac{2\Delta_n}{w_n}\frac{\Delta_n}{eFL}\right] , \quad r_n=(1-t_n^2)^{1/2} .$$

With $E_n=E_1n^2=\hbar^2\pi^2n^2/2mL^2$, the upper band edge of the nth level, we can define the bandwidth $w_n=\partial_n E_n=\hbar^2\pi^2 n/mL^2$. These results are derived for the Kronig-Penney model in Appendix B and their generalization to smooth potentials is straightforward. For the case of a weak potential $V(x)$ and/or high energies $\varepsilon_{n,\alpha}$, the assumption of completed Zener tunneling transitions is always fulfilled (for a more detailed discussion see Appendix B). Note that the amplitude for Zener tunneling is not an analytic function of the electric field.

The phases Θ_n and ϑ_n are

$$\Theta_n=\pi\left[\tau n^2+\frac{\Delta_n}{eFL}\right] ,$$
$$\vartheta_n=\chi_n+\frac{\pi}{2}\tau n\left[\left[1+\left[\frac{2\Delta_n}{w_n}\right]^2\right]^{1/2}+\left[\frac{2\Delta_n}{w_n}\right]^2\ln\left\{\frac{w_n}{2\Delta_n}+\left[1+\left[\frac{w_n}{2\Delta_n}\right]^2\right]^{1/2}\right\}\right] .$$

Here τ is the ratio between the unit of energy in the ring E_1 and the potential-energy drop eFL along the ring produced by the electric field: $\tau=E_1/eFL$. The physical meaning of the phases Θ_n and ϑ_n is illustrated in Fig. 1. Θ_n is the net change in phase due to the free-electron-like time evolution of the state between A and D, $\Theta_n=t_\pi(E_n+\Delta_n)/\hbar$. The first term in ϑ_n is a scattering phase χ_n for backscattering which in general depends on

the potential $V(x)$ and varies smoothly with the level index n (i.e., the energy). The second term in ϑ_n ($\sim n\tau\pi/2$ for large n) corrects for the phase due to the time evolution of the state when the particle is backscattered to C instead of forward to D.

As pointed out by Lenstra and van Haeringen, the phase Θ_n plays a key role for the time evolution of the system. The phase differences $\Theta_{n+1}-\Theta_n$ due to propagation in neighboring pairs of levels can become large, no matter how weak the field is, since $\partial_n\Theta_n=2\pi\tau n$ depends linearly on n. In general τ is an irrational number and therefore neighboring pairs of levels pick up random differences in phase for large n because τn modulo 1 is essentially a random number. The random phases Θ_n will lead to localization effects of the wave function in energy space as we will demonstrate in Sec. III. The phase ϑ_n is less important as χ_n varies continuously with n ($\chi_n>0$ increases monotonically to $\pi/4$ with increasing n for the Kronig-Penney model) and the second term is approximately linear in n.

For the lowest energy state $n=1$ there is no partner for scattering at $\alpha=2\pi l$ and we have to impose the boundary condition

$$c_1(\alpha_{2l})=e^{-i\Theta_0}c_1(\alpha_{2l-1}) ,$$

with $\Theta_0=\pi\tau/12$ for a free-electron-like band.

The S_n matrix is unitary because it describes a time evolution, and symmetric due to the time reversal symmetry $H(-t)=H^*(t)$. The time-reversal symmetry implies an equality for the time evolution of $\Psi(t)$ and $\Psi^*(-t)$. Therefore, the amplitudes for processes $\Psi_A\rightarrow\Psi_D$ and $\Psi_D^*\rightarrow\Psi_A^*$ must be equal, causing the off-diagonal elements of the S_n matrix to be identical. Furthermore, S_n does not depend on the time at which the scattering event takes place but only on the level index n of the lower band.

The matrix S_n takes the amplitudes $c_n(\alpha)$ a step forward in time, increasing α by π. However, it is obvious from Fig. 1 that the full period in α is 2π, corresponding to a time interval $t_{2\pi}=h/eFL$, the period of Bloch oscillations. It is natural to introduce the discrete time evolution operator T which takes the system forward in time by an entire period, from α_{2k} to $\alpha_{2(k+1)}$. At each time α_{2k}, $k=0,1,\ldots$, we define the basis

$$u_n^{(k)}=u_{n,\alpha_{2k}} ,$$

the coefficients

$$c_n^{(k)}=c_n(\alpha_{2k}) ,$$

and the wave function

$$\Psi^{(k)}=\Psi(\alpha_{2k}) .$$

The time dependence of the basis $u_n^{(k)}$ in the x representation is given by the phase shift

$$u_n^{(k)}(x)=(-1)^k e^{-i2\pi kx/L}u_n^{(0)}(x) .$$

The unitary operator T then acts on the wave functions in the following way:

$$\begin{aligned} &T\Psi^{(k)}=\Psi^{(k+1)} ,\\ &Tu_m^{(k)}=\sum_n (u_n^{(k+1)},Tu_m^{(k)})u_n^{(k+1)}=\sum_n T_{nm}u_n^{(k+1)} . \end{aligned} \tag{8}$$

The coefficients $c_n^{(k)}$ obey the recursion relation

$$c_n^{(k+1)}=\sum_m T_{nm}c_m^{(k)} , \tag{9}$$

This equation is very similar to Eq. (7). Indeed we can find the matrix elements T_{nm} by applying the recursion relation (7) twice on the amplitudes $c_n^{(k)}$, mixing first the amplitudes $c_{2m-1}(\alpha_{2k})$ and $c_{2m}(\alpha_{2k})$ with S_{2m-1} at $\alpha=(2k+1)\pi$, and afterwards the amplitudes $c_{2m}(\alpha_{2k+1})$ and $c_{2m+1}(\alpha_{2k+1})$ with S_{2m} at $\alpha=2(k+1)\pi$. The operator T couples a final state $u_n^{(k+1)}$ to four initial states $u_n^{(k)}$. An explicit form for the operator T, i.e., its representation in level basis T_{nm}, will be given in Sec. IV.

With this derivation of the discrete time evolution operator T, we have cast the problem of the time evolution of the system into the form of a scattering problem. The time evolution has been reduced to a discrete set of points and thereby becomes amenable to numerical studies. As a consequence the current in the simulations is sampled only at discrete time steps, therefore the presence of a steady current cannot be determined unambiguously since an oscillating current with a period equal to the sampling period looks like a constant (i.e., the problem of aliasing arises). This proviso should be kept in mind when we are going to present our results in the next section.

The recursion relations (9) for the amplitudes $c_n^{(k)}$ look like those of a tight-binding model. This is similar to the problem of quantum chaos in the periodically kicked rotor.[21] Indeed our model for the localization of wave functions in level space looks like the problem of localization of wave functions in angular momentum space for the kicked rotor. However, the quantum model to which it corresponds is a rotor periodically kicked in time by a *nonlocal* potential, so we have not tried to map our problem onto that work.

C. Quasienergy

Since the matrix T_{nm} in Eq. (8) is independent of time we can define a new basis $u_\omega^{(k)}$ at each point α_{2k} which evolves trivially in time, namely

$$Tu_\omega^{(k)}=e^{-i\omega}u_\omega^{(k+1)} . \tag{10}$$

The quantity ω is called the quasienergy and we refer to the $u_\omega^{(k)}$ as the quasienergy eigenstates. We assume that Eq. (10) defines a complete basis $u_\omega^{(k)}$ with ω in the range $[-\pi,\pi]$ at each point α_{2k}. For practical purposes we cast Eq. (10) into matrix form. Using the abbreviation

$$u_{n,\omega}=(u_n^{(k)},u_\omega^{(k)})=\int_{-L}^{0} dx[u_n^{(k)}(x)]^*u_\omega^{(k)}(x) ,$$

we find that Eq. (10) takes the form

$$(u_n^{(k+1)},Tu_\omega^{(k)})=\sum_m T_{nm}u_{m,\omega}=e^{-i\omega}u_{n,\omega} . \tag{11}$$

Note that $u_{n,\omega}$ is independent of time because k has dropped out of our defining equation (11).

If we expand the wave function Ψ into quasienergy eigenstates the time evolution of Ψ simplifies to

$$\Psi^{(k)}=\int_{-\pi}^{\pi} d\omega \frac{1}{2\pi} c_\omega e^{-i\omega k} u_\omega^{(k)} , \tag{12a}$$

with the amplitude c_ω given by the initial condition

$$c_\omega=\sum_{n=1}^{\infty} c_n^{(0)} u_{u,\omega}^* . \tag{12b}$$

We conclude that once we know the character of the eigenstates $u_\omega^{(k)}$ we also control the time evolution of the wave function Ψ. For instance, if the states $u_\omega^{(k)}$ are localized in level space n (i.e., $|u_{n,\omega}|$ decays exponentially in n) then $\Psi(t)$ will be localized, too. One way to examine the nature of the eigenstates $u_\omega^{(k)}$ is to determine the local density of states (LDOS): Using Eqs. (12a), (12b), and the initial condition $c_n^{(0)}=\delta_{n,n_0}$, we find

$$c_{n_0}^{(k)}=(u_{n_0}^{(k)},\Psi^{(k)})=\int_{-\pi}^{\pi} d\omega' \frac{1}{2\pi} |u_{n_0,\omega'}|^2 e^{-i\omega' k} ,$$

and by a simple Fourier transformation of the time evolution of the initial amplitude $c_{n_0}^{(k)}$, we obtain the desired LDOS,

$$\sum_{k=-\infty}^{\infty} c_{n_0}^{(k)} e^{i\omega k}=\int_{-\pi}^{\pi} d\omega' \frac{1}{2\pi} |u_{n_0,\omega'}|^2 \delta(\omega-\omega') \equiv \rho(n_0;\omega) . \tag{13}$$

The amplitudes for negative times are determined by the time-reversal symmetry, $c_{n_0}^{(-k)}=(c_{n_0}^{(k)})^*$. If the disturbance remains localized at long times, we expect the local density of states $\rho(n_0;\omega)$ to be a set of sharp peaks representing those localized states $u_\omega^{(k)}$ which are peaked near n_0 and therefore strongly couple to the initial disturbance. This provides a simple way to examine whether the solutions to the recursion relations remain localized in level space or not.

Once given the LDOS we can pick a value ω_p (for instance, at a peak) and filter out the corresponding eigenstate $u_{\omega_p}^{(k)}$,

$$u_{n,\omega_p}=\frac{1}{u_{n_0,\omega_p}^*} \sum_{k=-\infty}^{\infty} c_n^{(k)} e^{i\omega_p k} , \tag{14}$$

where the same initial condition $c_n^{(0)}=\delta_{n,n_0}$ has been used. Equation (14) gives us simple and direct numerical access to the eigenfunctions $u_\omega^{(k)}$.

Another quantity providing useful information on the system is the current $j(t)$ which is given by Eq. (5). For the general case including Zener tunneling the current becomes

$$j^{(k)}=j_0 \sum_{n=1}^{\infty} |c_n^{(k)}|^2 (-1)^{n-1}(n-\tfrac{1}{2}) ,$$

$$j_0=\frac{e\hbar\pi}{mL^2} .$$

For the approximations used in the derivation of the above equation, see Appendix B.

Having established the formalism used in this paper, we now go on with the presentation of our results for the three model calculations treating the cases of constant Zener tunneling amplitudes $t_n=t$, the Kronig-Penney model with $V(x)=V_0\delta(x)$ as studied previously by Lenstra and van Haeringen, and a third model with a smooth potential $V(x)$ mimicking a screened impurity.

III. MODEL SIMULATIONS

In this section we will examine three models for the Zener tunneling process in a 1D loop of wire. In each model we will examine some feature of the scattering matrices S_n [see Eq. (7)] and approximate certain parameters to learn how important they are. We will always use the same initial condition as Ref. 11, namely unit amplitude ($c_n^{(0)}=1$) in states $n=200$ and 201. The discrete time evolution of the system is then calculated by repeatedly applying the unitary time evolution operator T on the wave function Ψ (or equivalently by applying twice the scattering operators S_n and mixing alternating pairs of levels). Data on the current and the distribution of amplitudes in the various levels are retained during the iteration.

Some comments about the simulations should be made. The simulations were run for 4096 time steps $t_{2\pi}$, more than 40 times longer than in Ref. 11 (note that in Ref. 11 a time step is defined over the interval t_π, so our results extend over 8192 steps t_π). These long runs we found to be important because the long-time behavior often appeared only gradually. Test runs were performed to ensure that numerical roundoff did not affect the results. To check unitarity, we ran the simulation forward for 4096 steps, then ran it backward for the same time, and checked that the initial state was recovered. This showed that unitarity was preserved to machine precision (1 part in 10^{14}). Another test we used was to run the simulation forward, take the complex conjugate of the amplitudes, then continue to run the simulation. The subsequent time evolution was the time-reversed version of the initial simulation, explicitly showing the time-reversal symmetry of the Zener tunneling.[17] We show the current in one such simulation in Fig. 2. From these tests we find that the finite precision of the calculation affected in no significant way the results obtained, even over the longest runs.

The three models that we examined are (a) a system with constant transmission amplitudes $t_n=t$, but phases that vary with energy; (b) the Kronig-Penney model studied by Lenstra and van Haeringen; and (c) a system with gaps that close with increasing energy unlike the Kronig-Penney model. For quick reference we have labeled the figures with "CTA" for the model with constant tunneling amplitudes, with "KP" for the Kronig-Penney model, and with "SI" for the screened impurity model.

In each case we examine (i) the phase randomization

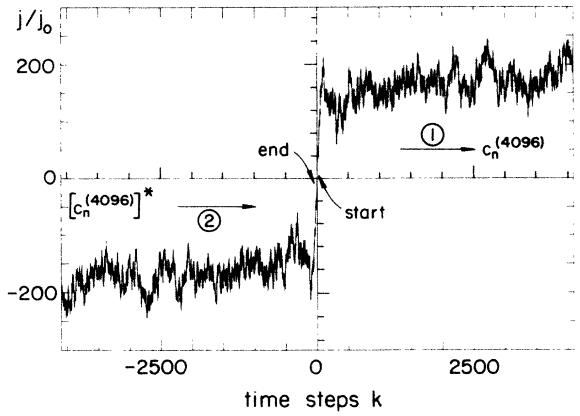

FIG. 2. Time reversal symmetry. With the levels 200 and 201 occupied at time $k=0$, the time evolution of the current $j^{(k)}$ is plotted for k between 0 (start) and 4096. The amplitudes $c_n^{(4096)}$ are then complex conjugated and used as the new initial condition at time $k=-4096$. Evolving the system again forward in time we recover the initial state at time 0 (end) with a precision of 1 in 10^{14}. This shows that the finite numerical accuracy of the simulation does not affect our results.

properties of the model, (ii) the behavior of the current as a function of time, (iii) the nature of the time-evolved state at long times, and (iv) the local density of modes that contribute to the initial disturbance.

A. Constant Zener tunneling amplitudes

The motivation for this model came from the claim by Lenstra and van Haeringen that the crucial feature of the Zener tunneling model was the apparently random phase that the wave function acquired while tunneling through different sequences of energy levels. To be more specific, consider Fig. 3. Here we show five different paths in energy space connecting points A and B at two different times. Whereas path (e) contributes an amplitude of order t^5r^1, the paths (a) to (d) all contribute terms of the same order $(tr)^3$ to the total amplitude at B. However all the latter four amplitudes arrive with different essentially random phases at B. Relative to the neighboring path, the phase differences are $\Theta_4-\Theta_2-(\partial_n^2\vartheta_n)_{n=3}$ between (b) and (a), $\Theta_5-\Theta_3-(\partial_n^2\vartheta_n)_{n=4}$ between (c) and (b), and $\Theta_6-\Theta_4-(\partial_n^2\vartheta_n)_{n=5}$ between (d) and (c).

Note that the phase ϑ_n usually is a very smooth slowly varying function of n, whereas the phases Θ_n are essentially random. Finally, adding up amplitudes with the same modulus but random phases leads to a strong suppression of the wave function at B. This is very similar to the phase randomization effects in Anderson's model of localization in a one-dimensional random potential.

Lenstra and van Haeringen then claimed that this phase randomization was the source of the constant current which they found to be proportional to the induced emf. We will therefore simplify the Zener tunneling so that the value of the tunneling probability t_n^2 between levels n and $n+1$ is independent of n (except for the boundary condition of the lowest level $n=1$). Furthermore, we drop the constant term in Θ_n and substitute the phase ϑ_n by $\vartheta_n=\pi\tau n/2$, such that the scattering matrix S_n takes the form

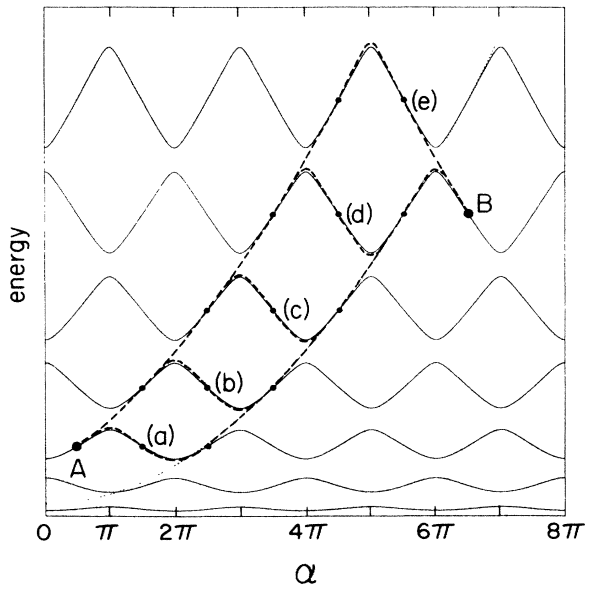

FIG. 3. Adiabatic energy levels $\varepsilon_{n,\alpha}$ as a function of flux α. We discuss the concept of phase randomization. The path (e) contributes a term of order t^5r^1 to the amplitude at B. All other four paths connecting points A and B contribute terms of the order $(rt)^3$; however, different paths pick up different phases. The phase differences between paths are approximately $\Theta_4-\Theta_2$ between (b) and (a), $\Theta_5-\Theta_3$ between (c) and (b), and $\Theta_6-\Theta_4$ between (d) and (c). Since the phases Θ_n are essentially random, the summation over different paths leads to a strong suppression of the total amplitude at point B.

$$S_n=e^{-i\pi\tau n^2}\begin{bmatrix} re^{-i(\pi/2)\tau n} & it \\ it & re^{i(\pi/2)\tau n}\end{bmatrix}. \tag{15}$$

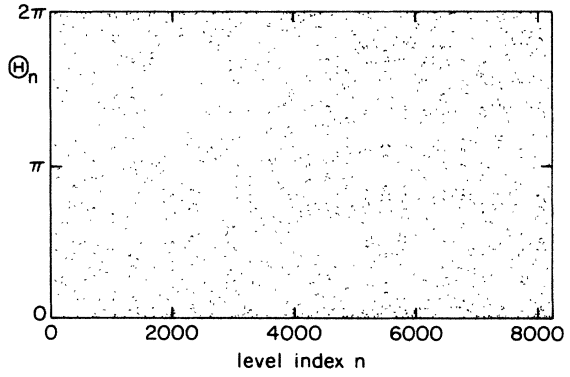

FIG. 4. Phase Θ_n picked up during a single forward scattering event as a function of level index n. The phase parameter $\tau=E_1/eFL$ has been chosen equal to the inverse of the golden mean $\tau_G=(1+\sqrt{5})/2$, $\tau=1/\tau_G$. The phases Θ_n are found by taking the modulus of $\pi\tau n^2$ with respect to 2π. The quasiperiodic patterns which appear on a large scale in n are due to close approximations of τ by a rational μ/ν, generating quasiperiods of length ν. Most important, however, is the locally random behavior of the phases Θ_n.

This simple form of S_n also lends itself to analytical treatment (see Sec. IV). The only parameter left in (15) in addition to the magnitude t of the tunneling amplitude is the phase parameter $\tau=E_1/eFL$. If τ is not a simple fraction like $\frac{1}{2}$ or $\frac{2}{3}$, the expression τn^2 modulo 2 acts like a random number generator and produces essentially random phases Θ_n as illustrated in Fig. 4. Here we have chosen τ equal to the inverse of the golden mean $\tau_G=(1+\sqrt{5})/2$, $\tau=1/\tau_G$. A quasiperiod ν (ν is an integer) in the pattern can be observed for those values of ν which lead to a good approximation of $\nu\tau$ by an integer number μ, $\tau\simeq\mu/\nu$. Although there is some regularity in the pattern on a large scale in n, the phase change locally is apparently quite random.

Keeping τ at this value, we have varied the tunneling amplitude t. The resulting current traces for four values of t are shown in Fig. 5. Note that t is quite close to one so that most of the time the particle will tunnel. For $0.7<t<0.9$ we found essentially the same behavior as shown in the bottom curve for $t=0.9$. As t drops below $1/\sqrt{2}$, backscattering starts to dominate. The Fourier transform of the current starts to show clearly resolved peaks. The number of peaks decreases as t approaches 0. This can be explained by the decrease of the number of levels involved in the time evolution of Ψ. As $t\to 0$ pure Bloch oscillations emerge.

The *short-time* behavior for t near to unity is essentially the same as seen by Lenstra and van Haeringen; however, the fluctuations are larger by a factor of 2 or 3 in our results. The behavior at *long time* is completely different from that seen in Ref. 11, since the mean current decays to zero even for $t=0.999$. We therefore conclude that the asymptotic behavior of this model is zero net current with large fluctuations. This is certainly one simple way for a steady state to be reached: Since the energy pumped into the system per unit of time is

$$\frac{dE(t)}{dt}=eFLj(t)$$

$[E(t)=(\Psi(t), H(t)\Psi(t))]$, the net energy exchange between the field and the system drops to zero, indicating that the particles have become localized in energy space. With a finite current such as reported by Lenstra and van Haeringen, the mean energy in the electronic degrees of freedom must increase linearly with time since we have no way to remove it from the electrons.[17]

Figure 6 shows the distribution of the probability $|c_n|^2$ in the levels n at the end of the run. Except for the top figure, there is little change in the distribution over the last 2048 time steps. While the state for $t=0.9$ appears to be localized over a narrow range of levels, the

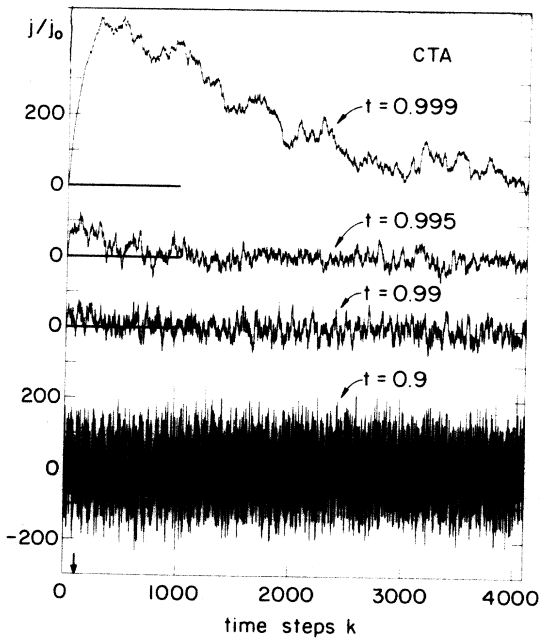

FIG. 5. Current j as a function of time for the model with constant Zener tunneling amplitudes $t_n=t$. k numbers the time steps $t_{2\pi}$. For $t=0.9$ the current evolution is characterized by large fluctuations around zero. As the tunneling amplitude t is increased, the current first rises and then relaxes back to zero. On average, no further energy is pumped into the system once it has attained its zero-mean-current asymptotic state. This state has not quite been reached for $t=0.999$. The arrow in the bottom left-hand corner marks the simulation time used in the work of Lenstra and van Haeringen, Ref. 11.

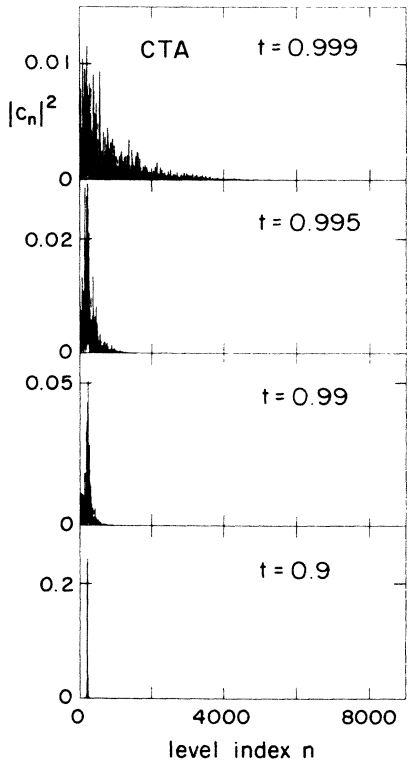

FIG. 6. Probability distribution $|c_n|^2$ after 4096 time steps $t_{2\pi}$ as a function of level index n. Except for the topmost figure ($t=0.999$) the distributions are essentially unchanged over the last 2048 time steps, in agreement with the observation that no further energy is pumped into the system after it has reached the zero-mean-current asymptotic state. The data strongly suggest that the wave functions become localized in energy space with a localization length which increases as the tunneling amplitude t approaches unity.

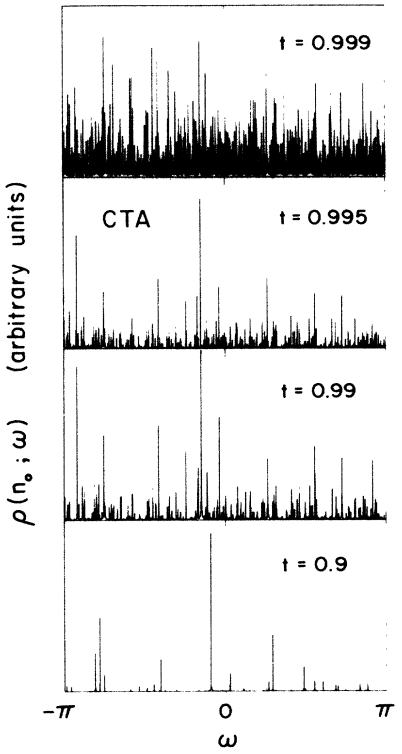

FIG. 7. Local density of states at the levels $n_0=200$ and 201 as a function of quasienergy ω. The spectrum appears pointlike for the case $t=0.9$ indicating that the quasienergy eigenstates are localized in energy space. Increasing the tunneling amplitude t leads to the filling in of additional peaks as more eigenstates overlap with the initial disturbance at levels 200 and 201. This indicates the increase of the localization length as t approaches unity. Note that the large peaks persist as t increases from 0.99 to 0.999. For $t=0.999$ the asymptotic state has not yet been reached.

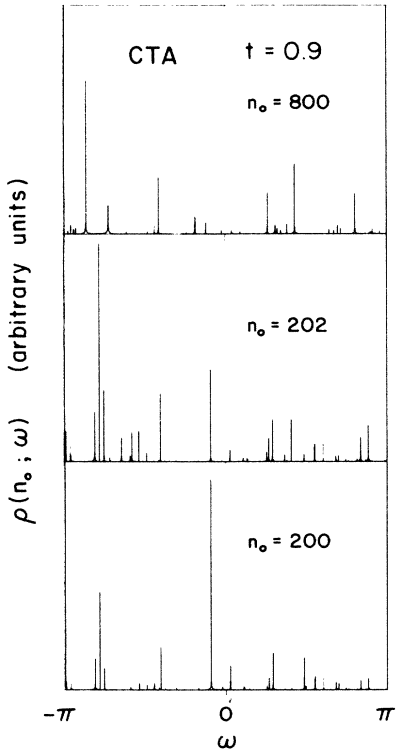

FIG. 8. Local density of states vs quasienergy ω at different positions in level space. The same peaks are present in the local density of states at $n_0=200$ and 202. Therefore, we conclude that the same localized quasienergy eigenstates contribute to these neighboring initial disturbances. As we move farther away from level 200 the local density of states changes completely. At level 800 different quasienergy eigenstates overlap with the initial disturbance and consequently the IDOS peaks at different values of ω.

localization evidently weakens as t approaches unity. This behavior is also reflected in the local density of states, shown in Fig. 7. For $t=0.9$ the spectrum clearly appears pointlike, which would occur if the eigenstates are localized. If the localization length were ξ, we would expect about ξ peaks in the LDOS. The two intermediate values of t clearly show the filling in of the density of states, indicative of decreasing localization. The interpretation of the $t=0.999$ results is ambiguous, primarily because the current has not returned to zero, indicating that we have not reached the asymptotic regime yet.

If our interpretation of the LDOS is correct, then neighboring pairs of levels should exhibit the same peaks in the LDOS with only the height of the peaks varying due to the slightly changed overlap of $u_{n_0}^{(k)}$ with the eigenfunctions $u_\omega^{(k)}$. This is indeed found to be true for the present model and is illustrated in Fig. 8, where we compare the LDOS for the level pairs (200, 201) and (202, 203). As we go farther away from our initial level $n_0=200$, we expect that other eigenfunctions $u_\omega^{(k)}$ will overlap with a specific site. Indeed, if we choose the pair (800, 801) the LDOS has changed completely as we show in Fig. 8.

The above arguments strongly suggest that the eigenfunctions $u_\omega^{(k)}$ of this particular system are localized in energy (level) space. We therefore have filtered out some eigenfunctions $u_\omega^{(k)}$ for the four values of t discussed above, using Eq. (14), and find that they are exponentially localized, indeed. The result is shown in Fig. 9 where we show a set of exponentially decaying eigenfunctions $u_{n,\omega}$ for the four values of t. Extracting the localization lengths ξ from the slopes, we find that the localization length diverges as t approaches unity and that the function $\xi(t)$ is well described by

$$\xi(t)\sim\frac{1}{1-t},\quad t\to 1\ . \tag{16}$$

Note that the parameter $1-t$ describes the deviation from free-electron–like acceleration, or, put into other words, is a measure for the scattering in the system. Of course our limited set of data can be described as well by $\xi(t)\sim 2/(1-t^2)$, which shows the same divergence as (16).

Thus we find that the process of phase randomization leads to localization of the wave functions in level space and therefore to *zero* average current asymptotically. A finite average current is incompatible with the localiza-

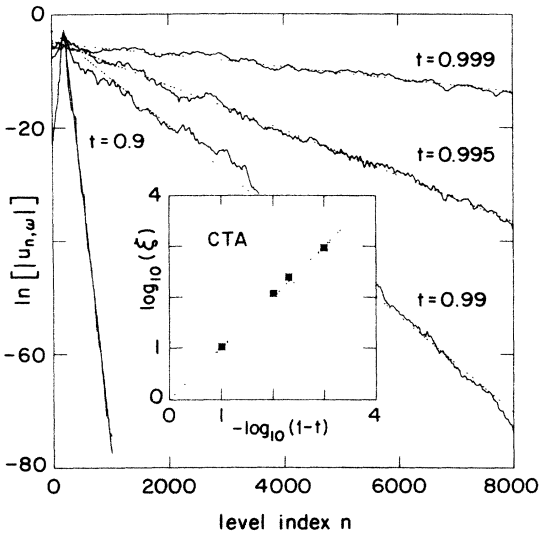

FIG. 9. Quasienergy eigenstates in level n representation are plotted vs level index n for four values of the tunneling amplitude t. An eigenstate belonging to a particularly prominent peak in the local density of states has been chosen in each case. Exponentially localized eigenstates are found and the localization length $\xi(t)$ is extracted from the slope of $\ln(|u_{n,\omega}|)$ vs n by linear regression. The inset shows the dependence of the localization length $\xi(t)$ on the tunneling amplitude t. The data are well represented by the form $\xi(t)=1/(1-t)$. The localization length ξ diverges as the tunneling amplitude t approaches unity.

tion of the wave functions as this requires the system to absorb energy continuously from the field. This can be achieved only if the wave function is delocalized, allowing the electrons to move up in level space.

The question may be raised if it is really the phase randomization which leads to the localization of the wave functions, or is it rather the exponential decay t^k of the leading edge of the wave function which is responsible for the localization? The answer to the second possibility is no. We will show in Sec. IV that if we substitute τ by a rational number, the eigenfunctions $u_\omega^{(k)}$ are extended in energy space. The above semiclassical view which neglects the phase is misleading.

Let us finally speculate on the role of the phase randomization. In his work Ping Ao[22] examines the behavior of the leading edge of the wave function in order to describe the time dependence of the current in the ring. Here we extend these ideas to discuss the behavior of the wave functions and to determine their asymptotic behavior at large energies.

For the present model we find that the leading edge of the wave function Ψ decays exponentially with increasing level index n, $|c_n| \sim t^n$. The tail, which this leading edge leaves behind, is decaying in the same way, like rt^n, since the particle is backscattered once. Having suffered a backscattering event, the amplitude now takes part in the phase randomization. Let us *assume* that the phase randomization localizes the wave function in energy space in the form of the tail left behind by the leading edge. The localized wave function then decays as t^n, or

$$|c_n| \sim t^n = \exp\left[-n \ln\left[\frac{1}{1-(1-t)}\right]\right]$$

$$\simeq \exp[-n(1-t)] ,$$

where the last equation applies for $t \to 1$. The localization length $\xi(t)$ then turns out to be $\xi(t)=1/(1-t)$, which is precisely the result we have found above. With our assumption, we can therefore reproduce our result for the asymptotic form of the wave function, and we find the correct dependence of the localization length ξ on the tunneling amplitude t.

B. Kronig-Penney model

The above discussion has shown that phase randomization together with constant Zener tunneling amplitude produces (i) exponentially localized wave functions in energy space, and (ii) zero asymptotic current. We now release the second condition and allow for the variation of the transmission coefficients t_n with level index n. In the case of the Kronig-Penney model discussed here, this variation is due only to the quadratic dispersion relation of the electrons as the gaps Δ_n are constant ($=\Delta$) and only the bandwidths (or velocities) w_n increase linearly with level index n.

As we have seen above that the localization length ξ diverges with t approaching unity, we might expect a weakening of the localization or even a delocalization of the wave functions at high energies where the transmission amplitudes approach unity. However, it is not clear that the resulting current asymptotically should approach a constant value as claimed by Lenstra and van Haeringen. Since it could be that the simulations of Ref. 11 were done over too short a time to see the asymptotic behavior, we have repeated the simulations on the Kronig-Penney model over a considerably larger time interval.

We have studied the behavior of the system for different values of the field strength F, as this is the experimentally accessible parameter. We chose a ring circumference $L=1$ μm and a scattering potential $V_0=10^{-12}$ eV m. This sets the interesting scale for the field (where $t_{200}>0.9$) to 1–10 V/m. We will illustrate our results for the values $F=1$, 3, 5, 7, and 9 V/m (in the following we will drop the unit V/m).

The phase parameter τ now depends on the strength of the field. In Fig. 10 we show the patterns for the phase Θ_n for our five field values. Again there is some varying degree of regularity on a larger scale in n and the length of the quasiperiods now change with the field. We have not found any structure in our results due to the existence of such quasiperiods, indicating that the randomness in Θ_n is enough to wash out correlations.

In Fig. 11 the current j is shown as a function of time. For weak fields $F \leq 1$ the behavior is very reminiscent of the $t=0.9$ behavior in the previous model, and the current for $F=3$ is very similar to that for $t=0.995$, where the current first increases and then returns slowly

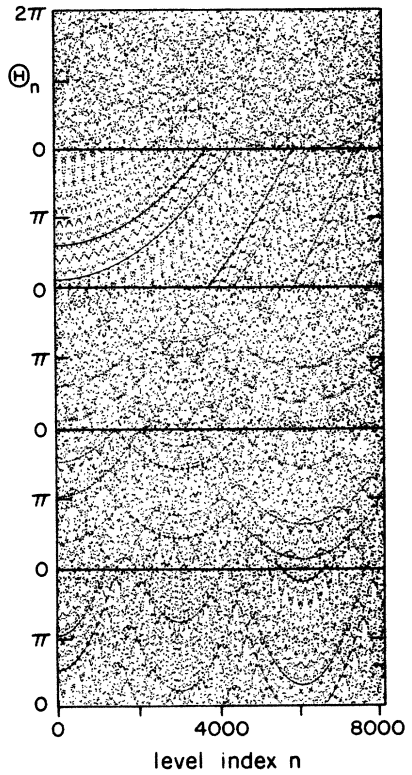

FIG. 10. Phase map Θ_n as a function of level index n for five different values of the electric field F; from top to bottom $F=9$, 7, 5, 3, and 1, respectively. Since the phase parameter $\tau=E_1/eFL$ depends on the field, the phase maps change with field. Quasiperiods appear when τ is well approximated by a rational μ/ν; the length of the quasiperiod is given by ν. Again the behavior of the phases Θ_n is essentially random on short scales.

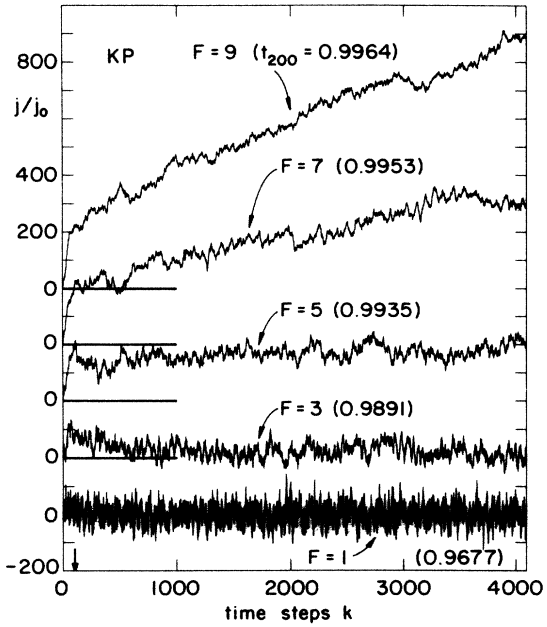

FIG. 11. Current j as a function of time for the Kronig-Penney model featuring asymptotically constant energy gaps. The traces for $F=1$ and 3 resemble the current evolution in the case of constant tunneling amplitudes, where the current relaxes back to a zero mean. For a field $F=5$ the current nearly saturates at a constant nonzero value. The presence of a linearly rising component in the current becomes evident as the field is further increased. This linearly increasing current indicates the presence of free-electron-like acceleration of a part of the wave function, i.e., the wave function seems to delocalize.

to a zero mean asymptotically. Thus for weak fields we see that the behavior looks very similar to that produced by phase randomization and constant Zener tunneling. We conclude that if the phase randomizing process produces a well-localized distribution, then the fact that the transmission probability varies with energy has only little effect. This view agrees well with the result found for the wave functions shown in Fig. 12. At low-field values the wave functions remain well localized at low energies. Similarly, the local density of states is pointlike as we expect it to be the case for a system characterized by localized wave functions, see Fig. 13.

As the field is increased, which means that the amplitudes t_n increase, we see a different behavior emerge. The current, which may remain nearly constant for a long time as in the $F=5$ case, eventually starts to increase linearly with time as we increase the field still further, indicating free-electron-like acceleration. Simultaneously, the wave function develops a long tail, headed by a pronounced peak, which decays only slowly for large fields. The system constantly picks up energy from the field to promote the particles to higher energies. The local density of states clearly fills in as the field strength is increased. Note that whereas in Fig. 7 new peaks are added to the already present peaks as t is increased ($t \geq 0.99$), here the LDOS changes completely as we increase the field F. The reason for this different behavior is given by the different generating function for the phases Θ_n: whereas the parameter τ did not depend on the transmission amplitude t in our model A, it depends on the field F in the case of the Kronig-Penney model.

Let us compare the results of our simulations with those obtained by Lenstra and van Haeringen. If we ignore the long-time behavior and examine the evolution only over the first 150 steps, then the current apparently saturates and becomes independent of time as reported by Lenstra and van Haeringen. On this short-time scale we then reproduce their results. However, as we follow the evolution over a longer time interval (4096 time steps) we have seen a completely different behavior emerge. Whereas for field values $F<5$ the current apparently saturates, we find a roughly linear increase of the current for larger fields. If we compare the saturation current $\langle j \rangle$ (over 4096 time steps) for field values $F \leq 5$ (where such a quantity may make sense) to the results of Lenstra and van Haeringen, we find that the average current $\langle j \rangle$ increases in size as the field is increased, see Fig. 14. However, it does not follow a linear law, and hence it is clear that this system does *not* show Ohmic behavior as has been claimed by Lenstra and van Haeringen. Note that the fluctuations in our simulation, which grow after the initial disturbance has felt the presence of the boundary at $n=1$, are much larger than in Ref. 11, where the simulation was stopped just as the disturbance reached $n=1$.

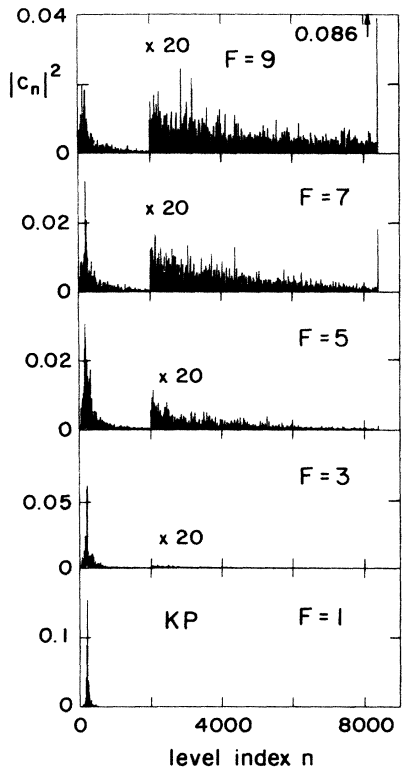

FIG. 12. Probability distribution $|c_n|^2$ after 4096 time steps $t_{2\pi}$ as a function of level index n. Whereas the wave functions look localized at low energies for field values $F=1$ and 3, the wave functions appear to be delocalized at high-field values $F=7$ and 9. In the latter two cases the ballistic peak at the leading edge moves linearly with time to the right, leaving a thin tail behind due to the very weak backscattering. The fraction of the wave function which is kept localized at low energies due to phase randomization decreases with increasing field.

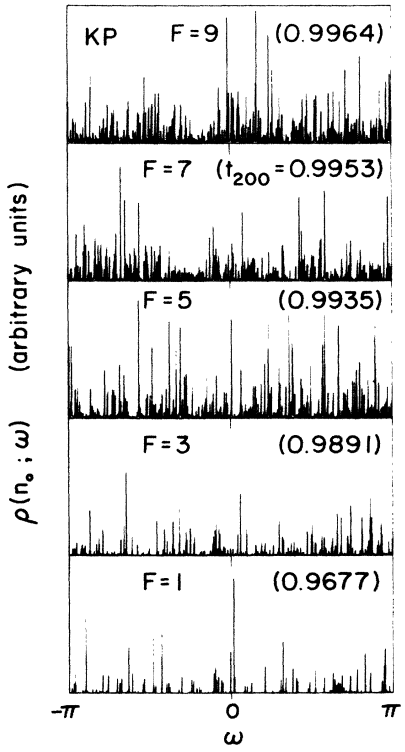

FIG. 13. Local density of states at levels $n_0=200$ and 201 as a function of quasienergy ω. Again the spectrum appears pointlike at low field values F. Increasing the field leads to the appearance of an increasing number of peaks in the spectrum. Contrary to the previous model discussing the case of constant tunneling amplitudes, here the large peaks shift with varying field. This is due to the dependence of the phase parameter τ on the field F.

Obviously it is very important to run the simulations over a long enough time interval in order to see the true asymptotic behavior of the system. How can we be sure then that we actually observe the right asymptotic behavior of the system? The answer is that at high fields we probably do *not* see it yet, in spite of our long simulation times. In the following we will repeat the analysis given at the end of the last section which was so successful in predicting the right answers for the model with constant Zener tunneling amplitudes.

We assume again that the phase randomization acts to preserve the form of the wave function as it is left behind by the leading edge. The Zener tunneling amplitudes t_n now depend on the level index n. We find the following asymptotic behavior of the amplitudes c_n:

$$|c_n| \sim r_n \prod_{l=n_0}^{n} t_l = (1-t_n^2)^{1/2} \exp\left[-\frac{1}{f}\sum_{l=n_0}^{n}\frac{1}{l}\right]$$
$$\simeq \left[1-\exp\left[-\frac{2}{f}\frac{1}{n}\right]\right]^{1/2} \exp\left[-\frac{1}{f}\ln\left[\frac{n}{n_0}\right]\right]$$
$$\propto \frac{1}{\sqrt{f}}\left[\frac{n_0}{n}\right]^{1/2+1/f},$$

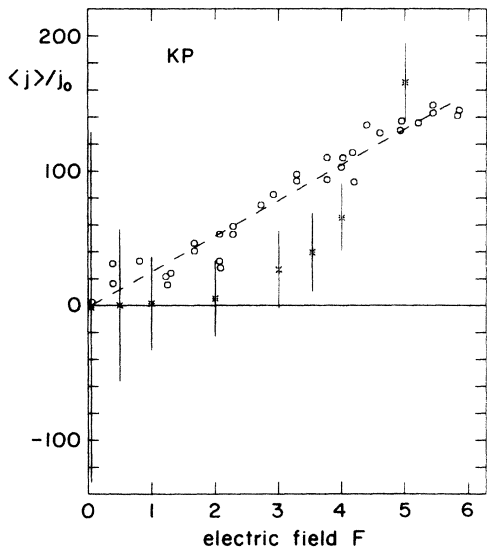

FIG. 14. Average current $\langle j\rangle/j_0$ over 4096 time steps $t_{2\pi}$ as a function of induced electric field F. We compare the results of our calculation (*) with those obtained by Lenstra and van Haeringen, Ref. 11 (○). The vertical bars represent the current fluctuations $\langle(j-\langle j\rangle)^2\rangle^{1/2}/j_0$. Whereas Lenstra and van Haeringen observe an Ohmic behavior, our data deviate largely from a linear relationship between the mean current and the induced field.

with

$$\frac{1}{f}=\frac{\pi^2}{4}\frac{\Delta}{E_1}\frac{\Delta}{eFL} . \tag{17}$$

Normalizing the wave function to unity we obtain the result

$$|c_n|=\frac{1}{\zeta\left[1+\frac{2}{f}\right]^{1/2}}\left[\frac{1}{n}\right]^{1/2+1/f},$$

where ζ denotes the Riemann ζ function.[23] This result then indicates that the wave functions Ψ and therefore also the quasienergy eigenfunctions for the Kronig-Penney model are *algebraically* localized for all field strengths. Numerical simulations again support this result: We have filtered out a few eigenfunctions numerically using again Eq. (14) and find that they are indeed decaying algebraically, see Fig. 15. For $F=1$ we find an exponent $\frac{1}{2}+1/f\simeq 5.7$ [the value expected from (17) is $\simeq 7.1$], for $F=3$ the result is $\frac{1}{2}+1/f\simeq 2.9$ [2.7 as expected from (17)], and for $F=5$ we find an exponent $\simeq 1.7$ (1.8 is the expected value, we have not quite reached the asymptotic region here as the current has not returned to zero). For higher-field values our simulations are probably far from reaching the asymptotic region.

If the wave functions are indeed algebraically localized we would expect that once the leading mode has decayed the current returns to zero asymptotically:

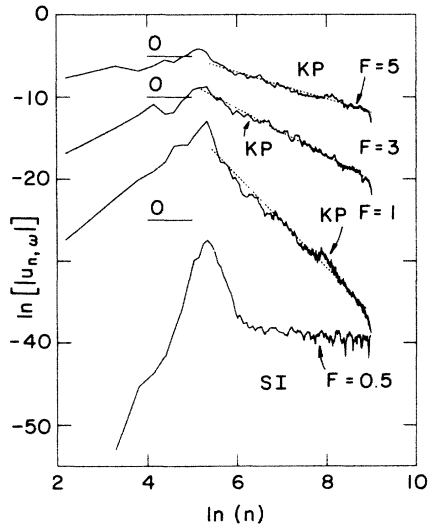

FIG. 15. Quasienergy eigenstates in level n representation vs level index n on a double logarithmic scale. Eigenstates belonging to particularly prominent peaks in the local density of states have been chosen. The eigenstates for the Kronig-Penney model decay algebraically with exponents $1/f+\frac{1}{2}\simeq 5.7$, 2.9, and 1.7 for increasing field values $F=1$, 3, and 5, respectively. The bottom curve illustrates the behavior of an eigenstate for the screened impurity model. Note the nearly constant tail developing above $n\simeq 400$.

$$\frac{j}{j_0}=\sum_{n=1}^{\infty}|c_n|^2(-1)^{n-1}(n-\tfrac{1}{2})$$
$$=\frac{1}{\zeta\left[1+\frac{2}{f}\right]}\left[\eta\left[\frac{2}{f}\right]-\tfrac{1}{2}\eta\left[1+\frac{2}{f}\right]\right],$$

with

$$\eta(s)=\sum_{n=1}^{\infty}(-1)^{n-1}\frac{1}{n^s} .$$

We then find that j/j_0 decays smoothly from $\frac{1}{2}$ to 0 as we increase the field, which is essentially zero on the scale of the fluctuations in the current which are always present. This relaxation to a zero mean current at long times can be observed in our simulations for the fields $F=1$ and 3. A check of the distribution of $|c_n|^2$ at field values $F\geq 5$ shows that we have not reached the asymptotic region as the leading mode of the wave function has not decayed yet, thus we cannot expect to see the current return to zero. Note that whereas the current returns always back to zero according to the above considerations, the total energy picked up by the system diverges if $f>1$ or $F>6.6$.

If we then trust the assumption concerning the role of the phase randomization made above, we have to conclude that (i) for the Kronig-Penney model the quasienergy eigenfunctions are algebraically localized, (ii) the current returns back to a zero mean asymptotically, and (iii) our simulation time is not long enough to observe the asymptotic behavior of the system at large fields: The linear rise we see is only a transient behavior.

C. Screened impurity model

A rather artificial feature of the Kronig-Penney model is the fact that the gaps remain constant at high energies. This is due to the sharpness of the potential $V(x)$, leading to a Fourier transform which behaves badly at infinity, i.e., the gaps do not close. We therefore investigated a third model where the δ function was replaced by a smooth scattering potential mimicking a screened impurity. The gaps in this model then shrink according to

$$\Delta_n=\frac{\Delta}{n^2+\kappa^2} .$$

The parameters Δ and κ were chosen such that for the 200th level the gap was the same as in the Kronig-Penney model and by the time the 500th level was reached the gap had been reduced to half its value at 200.

The changes in the phases Θ_n induced by the change in the potential are negligible, since almost all of the phase change is due to the kinetic energy. The current traces for the impurity model are shown in Fig. 16. We have chosen a field range which covers the typical low- and high-field behavior of this model, namely $F=0.5$, 1, 2, and 5. At low-field values $F<0.5$ the current strongly oscillates around a zero mean, the wave function which is shown in Fig. 17 appears localized, and the local density

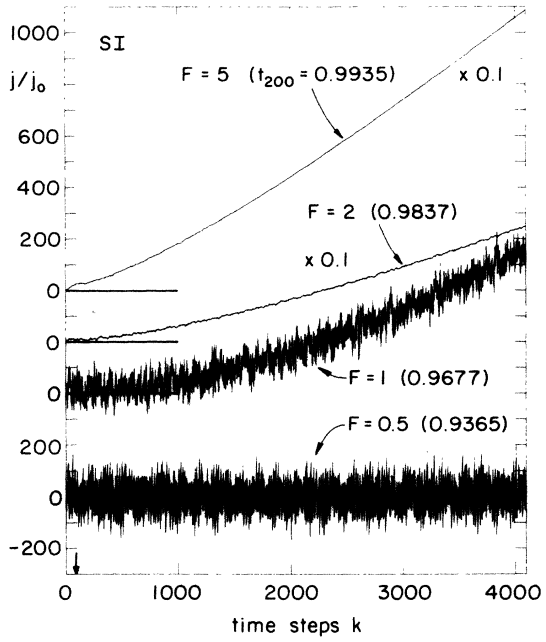

FIG. 16. Current j as a function of time for the screened impurity model which is characterized by asymptotically closing gaps. Similar to the Kronig-Penney model, the current fluctuates strongly around zero for a low-field value and increases in time as we go to larger electric fields. For field values $F \geq 1$ the current increases faster than linear, indicating that an increasing fraction of the wave function behaves free-electron-like as the time increases. Asymptotically the current has to attain a linear behavior.

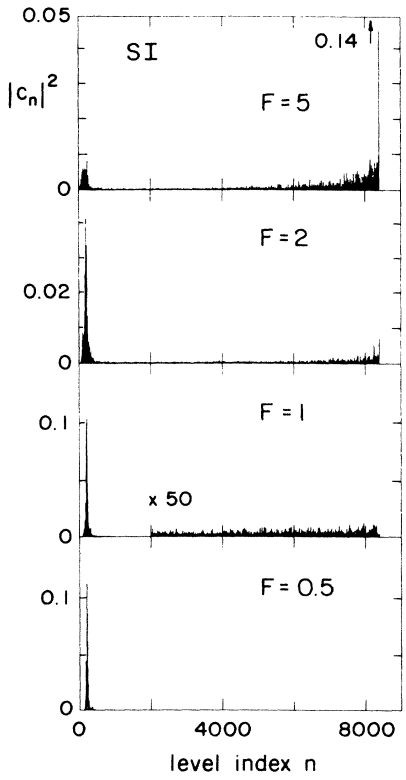

FIG. 17. Probability distribution $|c_n|^2$ after 4096 time steps $t_{2\pi}$ as a function of level index n. Again the wave function looks localized at low energies for the case of a weak applied field (bottom figure). At higher field values the wave functions develop a pronounced tail which looks very different from the tail developed by the wave functions for the Kronig-Penney model. This can be understood by noticing that the gaps shrink rapidly with increasing energy for the impurity model, such that the tunneling amplitude approaches unity much more rapidly. Note that the pronounced ballistic peak at high field values will attain a nonzero weight asymptotically.

of states is pointlike as shown in Fig. 18. Thus we find that at low-field values the system essentially behaves like the Kronig-Penney model. This can be understood by noticing that the gaps are fairly constant over the first 400 levels and therefore the tunneling amplitudes t_n show the same dependence on the level index n as in the Kronig-Penney model. The wave function then should become algebraically localized as long as it does not probe higher lying states, which is essentially the case at low enough fields as $F < 0.5$. This explains the behavior of the system as observed at low fields.

We point out, that since the wave function decays only algebraically, we cannot define a localization length. Therefore, there is always a thin tail of the wave function which probes levels at higher energies. This tail will delocalize and move up in energy space. We have filtered out a few quasienergy eigenstates for $F = 0.5$ and find that they decay algebraically up to $n \simeq 400$. For $n > 400$ a tail is observed which delocalizes to high energies, see Fig. 15. The amplitude in this tail, however, is strongly suppressed compared with the localized part of the wave function at low energies (a suppression of 10^{-5} is found in our numerical result for $F = 0.5$). The wave function is then not strictly localized but slowly leaks through its tail at large energies.

As we turn to higher-field values a different behavior is observed. By the time the field reaches 1 we can already see the runaway caused by the rapid increase in the transmission amplitudes t_n with level index n. Whereas the parameter γ_n [see Eqs. (B6) and (B7)] decays only as $1/n$ for the Kronig-Penney model and for the impurity model at low energies, it decays like $1/n^5$ for the impurity model at high energies. The leading mode of the wave function does not decay to zero any longer since the product of the tunneling amplitudes t_n converges to a finite value asymptotically.[22] This leading mode can be nicely observed in the figures for the probability density $|c_n|^2$ at large field values, see Fig. 17. With an asymptotically finite weight of the wave function in the leading mode the current then will never relax back to a zero mean.

Do we then have to conclude that localization effects due to phase randomization are not important in a real system where the gaps close with increasing energy? To answer this question we point out that for a field $F = 0.5$, where typically 90% of the particles tunnel, the effects of the phase randomization are drastic: the phase randomization very efficiently prevents the particles from running away to high energies and thereby suppresses the current

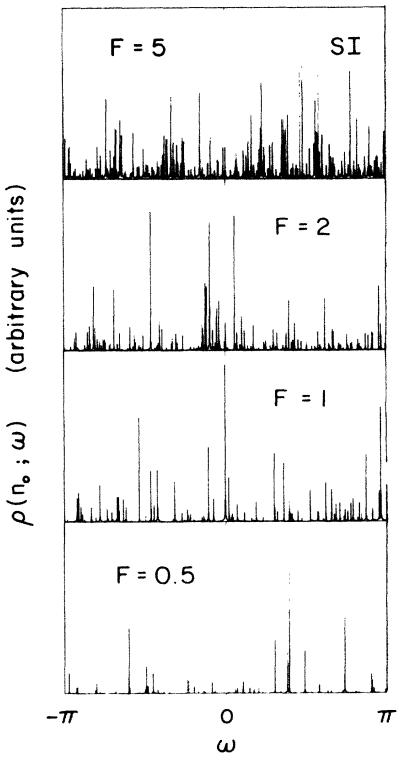

FIG. 18. Local density of states of levels $n_0=200$ and 201 as a function of quasienergy ω. The pointlike spectrum found for low electric fields (bottom figure) fills in as we increase the strength of the field F.

flowing in the ring.

We remark that since we find again a rapid crossover from localized to delocalized behavior as we increase the field, it is clear that a finite range potential $V(x)$ produces a highly non-Ohmic result, in agreement with arguments made by Landauer.[15]

In summary, the study of the above three models has led us to the following conclusions: (i) Phase randomization leads to localization of the wave functions, not to a constant current and Ohmic behavior as claimed by Lenstra and van Haeringen. (ii) For constant Zener tunneling amplitudes the current relaxes back to zero asymptotically and the wave functions are exponentially localized. (iii) For the Kronig-Penney model we expect algebraically localized eigenstates and a current which asymptotically returns to zero. This result is based on an assumption concerning the role of the phase randomization and we have presented some numerical evidence supporting it. (iv) If the tunneling amplitudes approach unity faster than for the Kronig-Penney model the wave functions delocalize and the current starts rising indefinitely with time.

Finally, it may be possible that the inclusion of the inelastic scattering will cause the distribution $|c_n|^2$ to change, as energy is transferred from the ring to some large reservoir, and the behavior we have seen above will be cut off. It is not clear if this will combine with Zener tunneling and produce Ohmic behavior for the current in a ring.

IV. PHASE RANDOMIZATION AND LOCALIZATION

In this section we will investigate the effects of phase randomization in detail. We will confine the discussion to the case of constant Zener tunneling amplitudes $t_n=t$. In Sec. IV A we will present some analytic results where we show that a system with no random phases is characterized by extended wave functions. As we increase the number of different phases in the system we find that the wave functions tend to become localized. This will be illustrated in Sec. IV B where we follow the behavior of the system as the phase randomization is gradually turned on. The results of the second subsection will be mainly numerical.

A. Periodic phases

We shall start from Eq. (15) which contains all essential features of the model. It is convenient to remove some of the phases in (15) by redefining the phases of the wave functions $u_n^{(k)}$,

$$u_n^{(k)} \rightarrow \tilde{u}_n^{(k)} = e^{i\eta_n} i^n u_n^{(k)} , \tag{18}$$

with

$$\eta_n = \sum_{l=1}^{n-1} \vartheta_l = n(n-1)\frac{\pi}{4}\tau .$$

We will drop the tilde in the following since we keep working in this basis from now on. Using the above unitary transformation we determine the discrete time evolution operator T by iterating the recursion relation (7) twice, mixing alternating pairs of levels as described in Sec. II. The matrix T_{nm} which defines the recursion relations for the amplitudes $c_n^{(k)}$,

$$c_n^{(k+1)} = \sum_m T_{nm} c_m^{(k)} ,$$

takes the simple form

$$T = e^{-i(\pi/2)\tau} VW ,$$

$$W = \begin{bmatrix} \ddots & & & 0 \\ & \begin{bmatrix} r_{2m} & t \\ -t & r \end{bmatrix} & & \\ & & \ddots & \\ 0 & & & \end{bmatrix} , \tag{19}$$

$$V = \begin{bmatrix} \ddots & & & 0 \\ & e^{-i2(2m)^2\pi\tau} & \begin{bmatrix} re^{-i4m\pi\tau} & te^{i2m\pi\tau} \\ -te^{-i2m\pi\tau} & r_{2m}e^{i4m\pi\tau} \end{bmatrix} & \\ 0 & & & \ddots \end{bmatrix} .$$

Here r_{2m} denotes the $2m$th element along the diagonal. The matrix T_{nm} couples $c_n^{(k+1)}$ to four amplitudes $c_n^{(k)}$. The unitary transformation (18) renders the matrix W real. The boundary condition for the lowest level $n=1$ leads to the recursion

$$c_1^{(k+1)} = e^{-i(\pi/12)\tau}(-tc_2^{(k)} + rc_1^{(k)}) . \tag{20}$$

Equations (19) and (20) completely determine the discrete time evolution of the system.

How can we manipulate the degree of phase randomization? As pointed out in Sec. II the phases Θ_n show a quasiperiodicity with a quasiperiod ν if τ is close to a rational μ/ν. If we deliberately pick a rational number for τ, $\tau=\mu/\nu$, then the phases Θ_n repeat exactly after going up 2ν levels in energy space. This is a sufficient, not a necessary condition, of course. Therefore, by setting the phase parameter τ equal to a rational number μ/ν, we introduce a unit cell in level space of length less or equal to 2ν. The task of calculating the spectrum and the eigenfunctions of the discrete time evolution operator T becomes identical to the problem of finding the vibrational eigenmodes of a half-infinite 1D chain of atoms with a unit cell containing 2ν different masses (or springs). The only difference is that T is a unitary operator whereas the phonon problem is characterized by a Hermitian operator. Therefore, the spectrum of T will be on the unit circle in the complex phase instead of on the real axis.

In the next section we will approximate the inverse of the golden mean $1/\tau_G$ by the sequence

$$\tau_n=\frac{x_n}{x_{n+1}}\ ,\quad x_{n+1}=x_n+x_{n-1}\ ,\quad x_0=x_1=1\ ,$$

using the Fibonacci sequence x_n. For the moment we will concentrate on the lowest approximants $\tau_0=1$ and $\tau_1=\frac{1}{2}$ as they can easily be treated analytically and provide insight into the behavior of the model without phase randomization.

Setting τ equal to 1 in (19) we obtain a particularly simple form for T since all the phases are 1. [We have dropped the uninteresting phase $\exp(-i\pi\tau/2)$ in Eq. (19) since this leads to a mere shift of the spectrum.] The size of the unit cell in level space is 2, the minimal possible size. We first solve the eigenvalue problem for the infinite system and take into account the boundary condition (20) later.

Our aim is to solve the eigenvalue problem (10), in matrix notation Eq. (11). Because of the periodicity in level index n it is useful to make a Fourier ansatz for $u_{n,\omega}$,

$$u_{n,\omega(q)}=\begin{cases}u_q^e e^{i2mq}\ , & n=2m\\ u_q^o e^{i(2m-1)q}\ , & n=2m-1\ .\end{cases}\tag{21}$$

Since we have two levels per unit cell we can restrict q to $[-\pi/2,\pi/2]$ and we expect to find two modes for each q value. Inserting (21) into Eq. (11) and using the simple form for T, we find the following eigenvalue equation for the polarization vector (u_q^e,u_q^o):

$$\begin{bmatrix}e^{-i\omega}-1-2it^2e^{iq}\sin(q) & 2i\sin(q)\\ 2i\sin(q) & e^{-i\omega}-1+2it^2e^{-iq}\sin(q)\end{bmatrix}\begin{bmatrix}u_q^e\\ u_q^o\end{bmatrix}=0\ .$$

The secular equation determines the dispersion relation $\omega(q)$ and we obtain the result

$$\omega(q)=\pm 2\arcsin(t\sin q)\ .\tag{22}$$

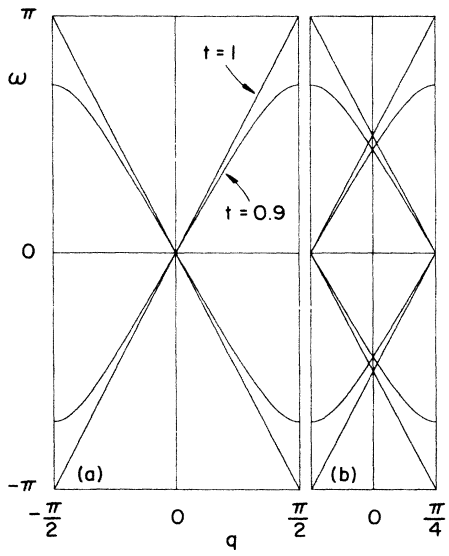

FIG. 19. Quasienergy ω as a function of wave number q for two models characterized by periodic phases Θ_n: (a) $\tau=1$, the size of the unit cell is 2. The dispersion is linear, $\omega=\pm 2q$, for $t=1$. As t decreases a gap opens in the spectrum which increases as t approaches 0. For $t\to 0$ the dispersion becomes linear again, $\omega\to 0$. (b) $\tau=\frac{1}{2}$, the unit cell size is 4. The new dispersion is found by shifting and back folding the dispersion in (a).

The dispersion $\omega(q)$ is shown in Fig. 19(a) for $t=0.9$ and 1.

The eigenvectors are determined by the ratio

$$r(q,\omega)=\frac{u_q^e}{u_q^o}=\frac{2tr\sin(q)}{\sin\omega+t^2\sin(2q)}\ .$$

$r(q,\omega)$ is positive (negative) for the branch with $\mathrm{sgn}(\omega)=\mathrm{sgn}(q)$ [$\mathrm{sgn}(\omega)=-\mathrm{sgn}(q)$], respectively.

In the limit $t\to 1$, Eq. (22) simplifies and we obtain the linear dispersion $\omega(q)=\pm 2tq$. The *extended* eigenstates $u_\omega^{(k)}$ then are traveling modes moving up or down through level space,

$$u_{\omega(q)}^{(k)}=\sum_n \delta_{n,o}e^{i(n-2k)q}\ ,\quad \omega=2q$$

$$u_{\omega(q)}^{(k)}=\sum_n \delta_{n,e}e^{i(n+2k)q}\ ,\quad \omega=-2q\ .$$

Here we have used the symbol $\delta_{n,o}(\delta_{n,e})$ which is 1 on odd- (even-) numbered levels and zero elsewhere, respectively. An initial disturbance therefore moves at a velocity $2t$ through level space without any dispersion.

As we decrease the tunneling parameter t three things happen: (i) a gap opens up in the quasienergy spectrum, (ii) the velocity of the long-wavelength modes decreases to $2t<2$, and (iii) modes with q near to the Brillouin-zone edges $\pm\pi/2$ show strong dispersion. Note that strong dispersion near the Brillouin-zone edge leads to a van Hove singularity in the density of states. In a comparison with phonon modes in a crystal the decrease of the tunneling amplitude t corresponds to an increase of the atomic mass in the crystal.

As the tunneling t approaches zero, we find again a dispersion-free propagation of the initial disturbance; however, the velocity in level space is zero, meaning that the particle remains in its initial level forever. This is the limit of Bloch oscillation.

Most important we find that the simplest model without phase randomization leads to *extended* quasienergy eigenstates $u_{\omega}^{(k)}$. This property is not specific to the case $\tau=\tau_0$—every model characterized by periodic phases Θ_n has extended eigenstates. However, as we will shortly see, the system approaches the quasiperiodic limit showing localized eigenfunctions smoothly as we increase the size of the unit cell. Note that as mentioned before in Sec. III, the rapid (exponential) decay of the amplitude for the leading edge of the wave function does not produce localized wave functions if no phase randomization is present.

A new feature appears as we include the boundary condition (20) into the model. To satisfy Eq. (20) we have to define new eigenstates $u_{\omega(q)}^{(k)}$ by superposing up-going and down-going states of the same energy $\omega(q)=\omega(-q)$, $q>0$, on opposite sides of the Brillouin zone,

$$u_{n,\omega(q)} \rightarrow u_{n,\omega(q)} + b_q u_{n,\omega(-q)} \ .$$

An interesting by-product is then the appearance of boundary states which decay exponentially as we move up in level space. A short look at Eq. (22) tells us that all boundary states appear at $q=\pm\pi/2$ and they decay in level space on a scale κ, where

$$\kappa=\cosh^{-1}\left[\frac{1}{t}\sin\left[\frac{\omega}{2}\right]\right] .$$

We then conclude that boundary states are found for $t<1$ at the edge of the Brillouin zone with a quasienergy ω in the gap $2\arcsin t < |\omega| < \pi$.

Having established this new formalism the interesting question is what happens as we increase the unit cell size by gradually approaching an irrational phase parameter τ? Of course, the most simple thing to do is to examine the case $\tau_1=\frac{1}{2}$. We can follow through the above formalism in exactly the same way, the only difference being that we now have to deal with a 4×4 matrix, since the size of the unit cell is now 4. It turns out that the dispersion relation $\omega(q)$ becomes

$$\omega(q)=\pm 2\arcsin\left[t\left[\begin{array}{c}\sin\left[q-\frac{\pi}{4}\right]\\ \cos\left[q-\frac{\pi}{4}\right]\end{array}\right]\right] .$$

As expected we find four branches within the Brillouin zone $[-\pi/4,\pi/4]$ and we show a plot of the dispersion in Fig. 19(b). It turns out that the dispersion is merely shifted and backfolded to the reduced Brillouin zone as compared to the τ_0 case. Therefore, nothing particularly interesting happens as we go from τ_0 to τ_1. However, very interesting results are found as we go beyond τ_1. As it becomes rather tedious to diagonalize the corresponding large matrices, we will investigate the system with the numerical tools we have already used in Sec. III. This also allows us to compare the result directly with the findings of Sec. III.

B. Approaching phase randomization

In the following we will study the behavior of the system as we approach full phase randomization by introducing an increasing number of different phases Θ_n into the problem, i.e., by increasing the size of the unit cell. We will approach the system with true phase randomization characterized by $\tau=1/\tau_G$ in four steps: The case $\tau_2=\frac{2}{3}$ allows us to make connection with the previous section, $\tau_4=\frac{5}{8}$ and $\tau_6=\frac{13}{21}$ describe the intermediate range, and with $\tau_8=\frac{34}{55}$ we approach the case of phase randomizaton pretty well already. The tunneling parameter $t=0.9$ is held constant throughout this study.

We start with the discussion of the current $j^{(k)}$ which is shown in Fig. 20. In all four cases characterized by periodic phases Θ_n we see a linear increase of the current with time which indicates free acceleration of the electrons. The slope of the current, however, decreases as we increase the size of the unit cell, as if the electrons would become heavier. Remembering the analysis of the previous section we can interpret this behavior in the following way: The linear rise of the current must be due to the nondispersive traveling modes $u_{\omega(q)}^{(k)}$ which describe that part of the wave function $\Psi^{(k)}$ which travels up in level space at a velocity $2t$. The slope in the current is then

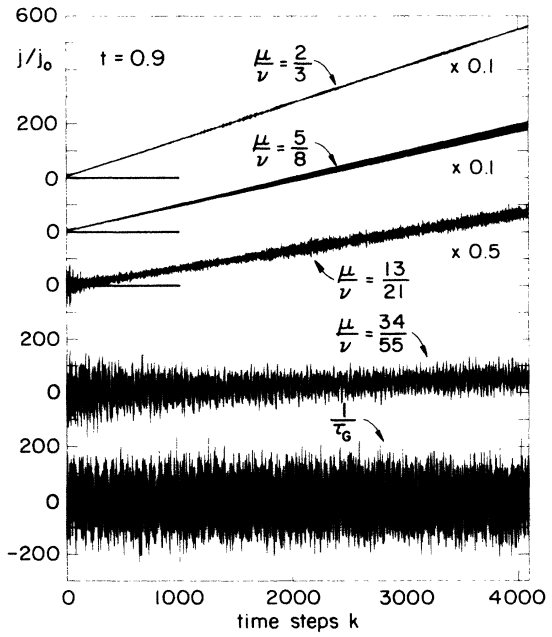

FIG. 20. Current j as a function of time for the model with periodic phases Θ_n. We compare the current for four examples characterized by periodic phases (top curves) with the current in the presence of full phase randomization (bottom curve). As we increase the size of the unit cell 2ν, the slope in the linear rise of the current is reduced, as if the electrons would become heavier.

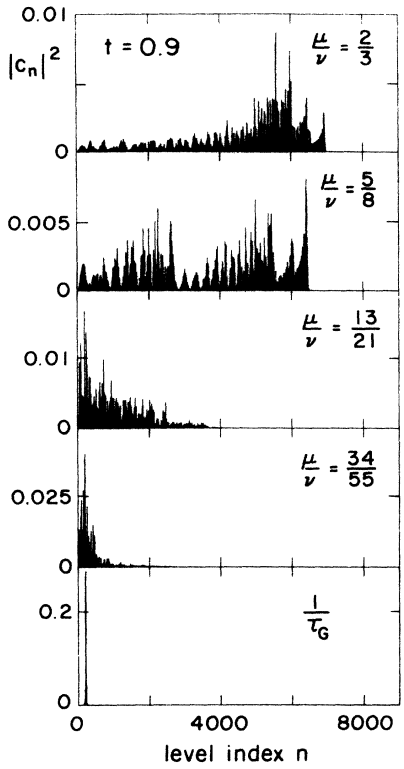

FIG. 21. Probability distribution $|c_n|^2$ after 4096 time steps as a function of level index n. As the size of the unit cell is increased following the figures from top to bottom the wave function Ψ seems to become localized. We point out, however, that the quasienergy eigenfunctions (and therefore also Ψ) are always extended if the size of the unit cell is finite. Only for the bottom wave function do we find an exponentially localized state due to phase randomization.

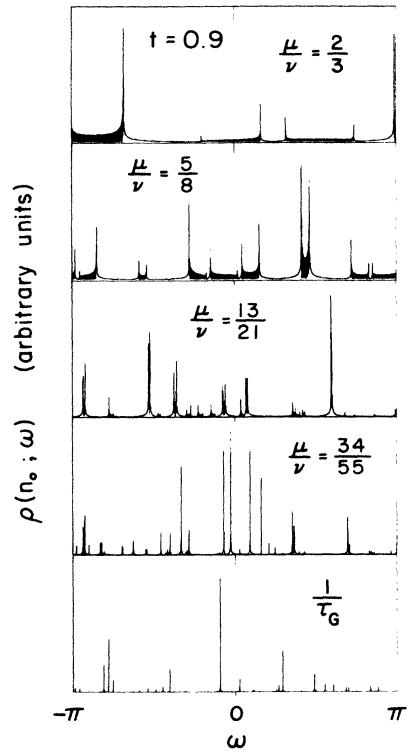

FIG. 22. Local density of states at the levels $n_0 = 200$ and 201 as a function of quasienergy ω. The LDOS for a small period ($\tau_2 = \frac{2}{3}$) shows 3 pronounced features: (i) a strongly oscillating behavior on the linear portions of the dispersion curve $\omega(q)$ which is due to the reflection from the boundary at $n = 1$, (ii) gaps are opening as the tunneling amplitude t decreases from unity, and (iii) van Hove singularities are marking the edges of the gaps. As the size of the unit cell is increased from top to bottom, the number of gaps increases and the weight of the spectrum is transferred from the linear portions in $\omega(q)$ to the van Hove singularities. As the unit cell becomes infinite for $\tau = 1/\tau_G$ the van Hove singularities have become the peaks marking the localized quasienergy eigenstates which overlap with the level n_0.

determined by the product of the velocity $2t$ and the fraction of the wave function which overlaps with these nondispersive traveling modes. Since the tunneling amplitude is constant in our five examples, the decrease in slope with increasing denominator ν indicates the disappearance of the nondispersive traveling modes. As we go beyond a unit cell size of 110 (τ_8), only the long-time behavior of the current allows us to distinguish between the cases of periodic phases Θ_n with a large unit cell and the fully phase randomizing case with an infinite unit cell.

In Fig. 21 we show the distribution $|c_n|^2$ at the end of the run. The beating structure observed for the cases $\tau = \tau_2$ and $\tau = \tau_4$ is due to the interference of different modes traveling through level space at nearly equal velocity. The leading edge of the wave function is never at $n = 8393$ as it is the case for the Kronig-Penney model and the impurity model in high fields: the origin of delocalization is different here. For $\tau = \tau_2$ the leading edge is roughly determined by the velocity $2t$ of the nondispersive traveling modes. As we go beyond τ_2 the maximal velocity for traveling waves obviously must decrease, since the leading edge of the wave function drops drastically. By the time we reach $\tau = \tau_8$ we see again that the wave function has become apparently localized at low energies.

The local density of states, which is shown in Fig. 22, is very helpful in understanding the behavior of the current and of the wave functions. Whereas essentially nothing changed when we increased τ_0 to τ_1 a new feature appears as we go beyond τ_1: The number of gaps in the spectrum increases with the size of the denominator ν in τ_n. In general, we find ν gaps for $\tau = \mu/\nu$ (for τ_7 we found only 17 instead of 34 gaps). The size of the gaps increases as the amplitude for Zener tunneling t decreases, as we have seen in the preceding section already. The LDOS shows the following three features.

(i) A strongly oscillating behavior is seen within the linear portion of the dispersion relation $\omega(q)$. This is most easily seen for the case $\tau_2 = \frac{2}{3}$, where the linear portions in the dispersion relation are still large. These oscillations are due to the standing waves created by the reflecting boundary at $n = 1$: Consider the simplest example of free traveling waves in a half-infinite lattice with a boundary condition $\Psi(0) = 0$. The eigenmodes are the functions $\sin(qn)$. The LDOS at $n = n_0$ is large for those

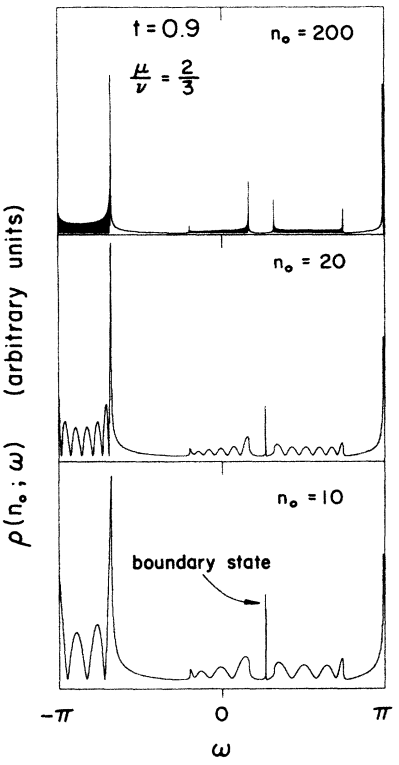

FIG. 23. Local density of states vs quasienergy ω at different positions in level space. The tunneling amplitude $t=0.9$ and the unit cell size 2ν are held constant. Following the figures from top to bottom we approach the boundary at $n=1$. The period of the oscillations in the LDOS due to the reflecting boundary grows like $1/n_0$. As we approach the lowest level an additional peak appears in the gap which marks the quasienergy of an exponentially decaying boundary state.

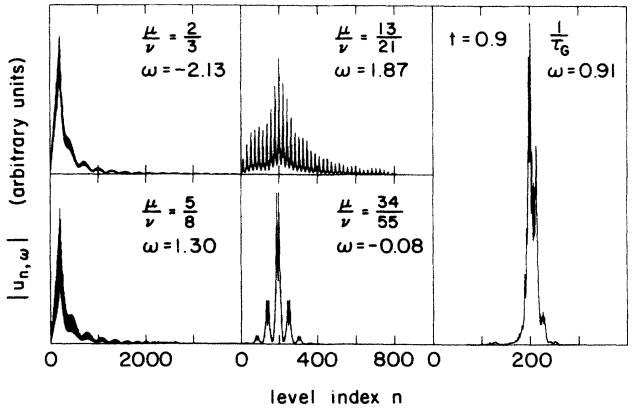

FIG. 24. Quasienergy eigenstates in level n representation are plotted vs level index n for four different sizes of a finite unit cell and for the case of an infinite unit cell. The tunneling amplitude $t=0.9$ is held constant. The smooth envelope modulating the extended eigenfunctions is due to the cutoff in the Fourier transform enforced by the finite simulation time. The pronounced spikes in the wave functions mark a region within the unit cell where the eigenfunction is large. The simulations suggest that these peaks within the unit cell become the exponentially localized eigenfunctions as the unit cell size is increased.

values of q which have a maximum at n_0 and small for those states having a node at n_0. The oscillations in the LDOS should therefore show a period proportional to $1/n_0$, and indeed they do, as we show in Fig. 23. Here we study the LDOS for different levels n_0 holding $\tau=\tau_2$ and $t=0.9$ fixed. Besides the above-mentioned change in oscillation, we also see the appearance of a boundary state in the gap as we approach the lowest level. When we filter out the corresponding eigenfunction with the help of Eq. (14), we find a boundary state which decays exponentially with a decay length of about 20 levels.

(ii) The number of the gaps increases with increasing size of the unit cell. [The LDOS does not drop to zero exactly because we have to cut off the Fourier transform in Eq. (13) due to our finite simulation time.] The fraction of 2π occupied by the increasing number of gaps increases, i.e., the measure of the spectrum decreases. Extrapolating to the case of the infinitely extended unit cell (full phase randomization), we expect to find a pure point spectrum of measure zero, which is typical for a system with exponentially localized wave functions.

(iii) The dominating features in the LDOS, finally, are the van Hove singularities which are created each time a new gap opens. All the weight of the spectrum goes into these peaks which then become the sharp peaks in the LDOS of the fully phase randomizing model showing localization of the wave functions. The linear portions of the dispersion $\omega(q)$ disappears gradually and their weight goes into the sharp peaks characteristic of strong dispersion. This explains how the particles apparently become heavier with increasing unit cell size, explaining the features observed in the current $j^{(k)}$ and in the distribution $|c_n|^2$.

The final question we may ask is how do the extended wave functions in the examples with a finite unit cell size approach the localized wave functions in the case of full phase randomization? To obtain an idea of what is going on we have filtered out some wave functions at the van Hove singularities for different sizes of the unit cell. The results are shown in Fig. 24 together with an example of a localized wave function for the case $\tau=1/\tau_G$.

The wave functions in Fig. 24 show two features. A spikey behavior on the scale of the unit cell and a smooth decay on a larger scale. The smooth decay is an artifact of our numerical filter which operates in ω space. At the location of a van Hove singularity, the density of states $dq/d\omega$ diverges and therefore a good filter in ω space of width $\Delta\omega$ is always a bad filter in q space, since $\Delta q \simeq \Delta\omega(dq/d\omega)$. Therefore, by probing states over the range Δq we pick up a shape function of width $\Delta n \sim \pi/\Delta q$ which modulates the infinitely extended eigenfunctions.

We then have to concentrate on the spikey structure within a unit cell. The picture which emerges from our simulations is the following: The eigenfunctions at the van Hove singularities peak strongly somewhere within the unit cell. Only those states contribute to the LDOS

which have their peak in the unit cell matching up with the probed state n_0. As we increase the size of the unit cell, the neighboring peaks move away and we remain with what will become the exponentially localized state. So the localized eigenfunctions develop out of a sharp peak within the unit cell of the extended eigenfunctions for the periodic case.

In this section we have shown how important a role the phase plays in this system. Let us therefore terminate this section by briefly considering the opposite limit of a classical model characterized by probabilities $p_n^{(k)}$ instead of amplitudes $c_n^{(k)}$, therefore lacking any phase. In such a model, particles are either transferred with probability t to the neighboring band or proceed within the same band with probability r, where now $t+r=1$. The time evolution of the probability distribution $p_n^{(k)}$ is then determined by a stochastic[24] matrix T which is again found by iterating twice the mixing of probabilities at each level approach.

Since there are no phases, the problem has a minimal unit cell of size 2 and we can repeat the analysis above for the case $\tau=\tau_0$. The eigenvalue equation for the polarization vector (p_q^o, p_q^e) now reads

$$\begin{bmatrix} e^{-\omega}-r^2-t^2e^{2iq} & -2rt\cos q \\ -2rt\cos q & e^{-\omega}-r^2-t^2e^{-2iq} \end{bmatrix} \begin{bmatrix} p_q^e \\ p_q^o \end{bmatrix} = 0 ,$$

with $r, t>0$, $r+t=1$. The eigenvalues are given by

$$e^{-\omega}=(r^2+t^2\cos 2q)\pm[(r^2+t^2\cos 2q)^2-(r^2-t^2)^2]^{1/2} .$$

For the long wavelength modes ($q\to 0$) we find the simpler expressions $1-q^2t/r$ and $(r-t)(1+q^2t/r)$. Since all modes with eigenvalues less than one decay exponentially in time, we end up with a diffusive behavior determined by the eigenvalue $1-q^2t/r$: after k steps the corresponding long-wavelength modes decay like

$$e^{-k\omega}=e^{-q^2(t/r)k} .$$

[Note the quadratic dispersion $\omega(q)$.] Fourier transforming to real space we finally find that an initial disturbance decays diffusively,

$$p_n^{(k)} \simeq \left[\frac{1}{\pi \mathcal{D}k}\right]^{1/2} e^{-[(n-n_0)^2/4\mathcal{D}k]} ,$$

with a diffusion constant $\mathcal{D}=t/r$. We thus obtain a completely different behavior for the classical and the quantum-mechanical systems characterized by either periodic or quasiperiodic phases Θ_n.

V. SUMMARY AND CONCLUSION

In this paper we have studied the single-particle properties of an electron in a small conducting ring subject to a constant electric field F which is generated by a linearly ramped magnetic flux. We have introduced the adiabatic eigenenergies $\varepsilon_{n,\alpha}$ and the corresponding eigenstates $u_{n,\alpha}$ which define a complete orthonormal basis set at every point in time. As the strength of electric field F is increased, transitions between the adiabatic eigenstates become possible.

To account for these transitions we have reformulated the problem of the time evolution and cast it into the form of a scattering problem. This was accomplished by integrating the time evolution of the system over one basic scattering event during which the particle can either tunnel to the neighboring state or be backscattered to its initial state. As a result, the time evolution of the system was reduced to a discrete set of points in time and thereby became amenable to numerical treatment. The time evolution of the system is determined by an operator T which takes the system forward in time by $t_{2\pi}$, the period of Bloch oscillations. We have introduced the notion of the quasienergy ω and the corresponding eigenfunctions u_ω which diagonalize the unitary operator T and constitute another complete basis set. Whereas the basis $u_n^{(k)}$ is useful to visualize the wave function Ψ, the basis $u_\omega^{(k)}$ is useful for understanding the asymptotic behavior of the system in time.

Having established the formalism, we have investigated the behavior of several model systems. To study the effect of phase randomization we have set the tunneling amplitudes t_n to a constant value t. We then have analyzed a model where the phases Θ_n picked up over one half-period t_π are quasirandom as we move through level space n. We have found that the quasienergy eigenfunctions for this model are exponentially localized in energy space. Since every solution $\Psi(t)$ of the Schrödinger equation can be represented as a linear superposition of these quasienergy eigenstates, we find that $\Psi(t)$ has to be localized in energy space, too. As a consequence the current carried by a state $\Psi(t)$ has to reach a zero mean asymptotically, since no net energy can be pumped into the system once the wave function has attained its (localized) asymptotic form.

To investigate the role of phase randomization further, we have studied a model where the phases Θ_n are not quasiperiodic but periodic (with a period p) in level space, $\Theta_{n+p}=\Theta_n$. For this model we have obtained extended quasienergy eigenfunctions and a current rising linearly in time. As the length p of the unit cell in energy space is increased, the quasienergy spectrum develops an increasing number of gaps and the weight of the spectrum is transferred to the van Hove singularities which separate allowed from forbidden regions of quasienergy ω. Simultaneously, the eigenfunctions corresponding to quasienergies at the van Hove singularities develop a sharp peak within the unit cell. Studying the behavior of the system when increasing the period p we could observe how the phase randomization tends to localize the eigenfunctions. As $p\to\infty$ we conjectured that the quasienergy spectrum becomes pure point and the peaks of the eigenstates within the unit cell develop into the exponentially localized states.

The second important set of parameters are the tunneling amplitudes t_n. To investigate the effects of their dependence on level index n on the single-particle properties of the system, we have studied two models. For the Kronig-Penney model the n dependence of the amplitudes is due to the quadratic dispersion relation of the (nearly free) electrons alone. The amplitudes t_n slowly

approach unity as we move up in level space. As a consequence we found indications for algebraically localized quasienergy eigenstates and again zero-mean asymptotic current. The asymptotic behavior of the system, however, is reached much more slowly than for the model with constant tunneling amplitudes.

As a more realistic model we have treated the case of a screened impurity potential which leads to gaps which close asymptotically. The tunneling amplitudes t_n then approach unity much faster than for the Kronig-Penney model where the gaps are asymptotically constant. For this model we have found delocalized wave functions which can move up in level space indefinitely. The current therefore increases with time and the system continuously absorbs energy from the electric field. However, also for this more realistic model we have found that the process of phase randomization is very important as it prevents a large fraction of the wave function from moving up ballistically in level space. To complete the analysis we have also studied a classical model and have found a diffusive behavior for the propagation of the probability distribution in energy space.

In this paper we have concentrated on the single-particle properties of the system. An important extension of this theory will be the incorporation of the fermionic nature of the electrons. As we want to describe realistic structures it also becomes important to take into account the finite number of transverse channels which are occupied in a wire of finite width. We also neglected effects due to inelastic scattering which may affect the transport properties in a real system. Since inelastic scattering tends to randomize the phases further and extracts energy from the electronic degrees of freedom, the combined effects of the phase randomization and (even weak) inelastic scattering are expected to prevent the electrons from attaining large energies in the electric field.

A technologically interesting problem to study is the transport properties of electrons in a semiconductor superstructure in strong electric fields where Zener tunneling between the minibands has to be expected. In this system the analysis then is complicated by the formation of "Stark ladders."[25]

The main conclusion which we draw from our study is that the process of phase randomization leads to localization effects and not to Ohmic or resistive behavior. This result is in agreement with the fact that a particle in a ring constitutes a Hamiltonian system for a single degree of freedom.

ACKNOWLEDGMENTS

We wish to thank Gunnar Eliasson, John Davies, Baruch Horovitz, Yu Kuang Hu, Alain Pumir, Dan Sullivan, Erkki Thuneberg, John W. Wilkins, and Ned Wingreen for helpful discussions. This work (of G.B.) was supported by the U.S. Office of Naval Research under Grant No. N00014-80C-0489 and (of D.B.) by the National Science Foundation (Division of Materials Research) under Grant No. DMR-84-17555.

APPENDIX A

In this appendix we briefly derive the energies and wave functions for the adiabatic limit of the ring problem, using a δ-function scattering potential $V(x)$ as our model potential. The eigenfunctions $\varphi_{n,\alpha}(x)$ are most easily determined by a transfer-matrix method.[26] Defining

$$\varphi^{<}_{n,\alpha}(x)=a_{n,\alpha}e^{iK_{n,\alpha}x}+b_{n,\alpha}e^{-iK_{n,\alpha}x},$$
$$\varphi^{>}_{n,\alpha}(x)=A_{n,\alpha}e^{iK_{n,\alpha}x}+B_{n,\alpha}e^{-iK_{n,\alpha}x}$$

to describe the wave function $\varphi_{n,\alpha}(x)$ on the left ($\varphi^{<}_{n,\alpha}$) and right-hand side ($\varphi^{>}_{n,\alpha}$) of the scattering potential $V(x)=V_0\delta(x)$, we can use the continuity condition $\varphi^{<}_{n,\alpha}(0)=\varphi^{>}_{n,\alpha}(0)$ and the condition

$$(\partial_x\varphi^{>}_{n,\alpha})(0)-(\partial_x\varphi^{<}_{n,\alpha})(0)=\frac{2mV_0}{\hbar^2}\varphi^{>}_{n,\alpha}(0) \tag{A1}$$

to relate the amplitudes $A_{n,\alpha}$ and $B_{n,\alpha}$ to the amplitudes $a_{n,\alpha}$ and $b_{n,\alpha}$ via the transfer matrix $T_{n,\alpha}$,

$$\begin{bmatrix}A_{n,\alpha}\\B_{n,\alpha}\end{bmatrix}=T_{n,\alpha}\begin{bmatrix}a_{n,\alpha}\\b_{n,\alpha}\end{bmatrix}$$
$$=\begin{bmatrix}1-i\dfrac{v}{K_{n,\alpha}L} & -i\dfrac{v}{K_{n,\alpha}L}\\ i\dfrac{v}{K_{n,\alpha}L} & 1+i\dfrac{v}{K_{n,\alpha}L}\end{bmatrix}\begin{bmatrix}a_{n,\alpha}\\b_{n,\alpha}\end{bmatrix}. \tag{A2}$$

Here $v=mV_0L/\hbar^2$, $\varepsilon_{n,\alpha}=\hbar^2K^2_{n,\alpha}/2m$, and (A1) is found by integrating Eq. (4a) over the interval $[-\varepsilon,\varepsilon]$ in real space. $T_{n,\alpha}$ has all the properties of a transfer matrix, $T_{22}=T^{*}_{11}$, $T_{21}=T^{*}_{12}$, $\det T=1$, and due to the symmetric potential $\mathrm{Re}T_{12}=0$.

The Bloch condition Eq. (4b) relates $\varphi_{n,\alpha}$ and its derivative at $x=L$ [i.e., $\varphi^{>}_{n,\alpha}(L)$ and $(\partial_x\varphi^{>}_{n,\alpha})(L)$] to the corresponding quantities at $x=0$ [i.e., $\varphi^{<}_{n,\alpha}(0)$ and $(\partial_x\varphi^{<}_{n,\alpha})(0)$], and we obtain the second condition

$$\begin{bmatrix}A_{n,\alpha}\\B_{n,\alpha}\end{bmatrix}=M_{n,\alpha}\begin{bmatrix}a_{n,\alpha}\\b_{n,\alpha}\end{bmatrix}$$
$$=\begin{bmatrix}e^{i(\alpha-K_{n,\alpha}L)} & 0\\ 0 & e^{i(\alpha+K_{n,\alpha}L)}\end{bmatrix}\begin{bmatrix}a_{n,\alpha}\\b_{n,\alpha}\end{bmatrix}. \tag{A3}$$

The Schrödinger equation (A2) together with the boundary condition (A3) determine both the spectrum $\varepsilon_{n,\alpha}$ and the eigenfunctions $\varphi_{n,\alpha}(x)$. The spectrum is found as usual by requiring that the matrix equation

$$(T_{n,\alpha}-M_{n,\alpha})\begin{bmatrix}a_{n,\alpha}\\b_{n,\alpha}\end{bmatrix}=0 \tag{A4}$$

has a nonvanishing solution, $\det(T_{n,\alpha}-M_{n,\alpha})=0$, leading to the implicit equation for $K_{n,\alpha}$,

$$\cos\alpha=\cos(K_{n,\alpha}L)+\frac{v}{K_{n,\alpha}L}\sin(K_{n,\alpha}L). \tag{A5}$$

With $(\alpha, K_{n,\alpha})$, a solution of (A5), all the combinations $(\pm\alpha, \pm K_{n,\alpha})$ are solutions, too. The upper band edges are determined by $LK_{n,\alpha}=n\pi$, $\alpha=0,\pi$. The allowed energy states are given by values $LK_{n,\alpha}\leq n\pi$, and the gaps in the spectrum correspond to values of $LK_{n,\alpha}$ slightly larger than $n\pi$, see Fig. 25. For a weak scattering potential V_0 the solutions for $LK_{n,\alpha}$ away from the Brillouin-zone edges $n\pi$ are approximately given by $LK_{n,\alpha}\simeq(n\pi-\alpha)$, $n=1,2,\ldots,\alpha\in[0,\pi]$.

The wave functions $\varphi_{n,\alpha}(x)$ are determined by the eigenvectors of (A4) which satisfy

$$\frac{b_{n,\alpha}}{a_{n,\alpha}}=\frac{iK_{n,\alpha}L}{v}\left[e^{i(\alpha-K_{n,\alpha}L)}-1+i\frac{v}{K_{n,\alpha}L}\right].$$

Normalizing $\varphi_{n,\alpha}(x)$ to 1 and choosing $\varphi_{n,0}(x)$ to be real we find the Bloch waves $(0\leq\alpha\leq\pi)$

$$\varphi_{n,\alpha}(x)=N_{n,\alpha}i^{(n-1)}(e^{i\mathcal{K}_{n,\alpha}[x+(L/2)]}-q_{n,\alpha}e^{-i\mathcal{K}_{n,\alpha}[x+(L/2)]}), \quad \text{(A6)}$$

with

$$q_{n,\alpha}=\frac{1}{\sin\delta_{n,\alpha}}[\sin(K_{n,\alpha}L+\delta_{n,\alpha})-\cos\delta_{n,\alpha}\sin\alpha],$$

$$LN_{n,\alpha}^2=\frac{1}{1+q_{n,\alpha}^2-2q_{n,\alpha}\dfrac{\sin K_{n,\alpha}L}{K_{n,\alpha}L}},$$

and

$$\tan\delta_{n,\alpha}=-\frac{v}{K_{n,\alpha}L}, \quad \mathcal{K}_{n,\alpha}=(-1)^{n-1}K_{n,\alpha}, \quad K_{n,\alpha}>0.$$

The eigenfunctions in the region $-\pi\leq\alpha\leq 0$ are obtained by complex conjugation,

$$\varphi_{n,-\alpha}(x)=\varphi_{n,\alpha}^*(x), \quad 0\leq\alpha\leq\pi.$$

For even-band indices n, $q_{n,\alpha}$ starts out with a value 1 for $\alpha=0$, drops near to zero in the middle of the band $(\alpha=\pi/2)$ and goes back to 1 as α approaches π. For odd-band indices the sign of $q_{n,\alpha}$ is reversed. The normalization constant $LN_{n,\alpha}^2$ starts out at $\frac{1}{2}$ $(\alpha=0)$, approaches 1 as $\alpha\simeq\pi/2$, and drops back to $\frac{1}{2}$ at the Brillouin-zone edge $\alpha=\pi$. This completes the description of the eigenvalues $\varepsilon_{n,\alpha}$ and eigenfunctions $\varphi_{n,\alpha}$ for the case of a δ-function scattering potential in the ring.

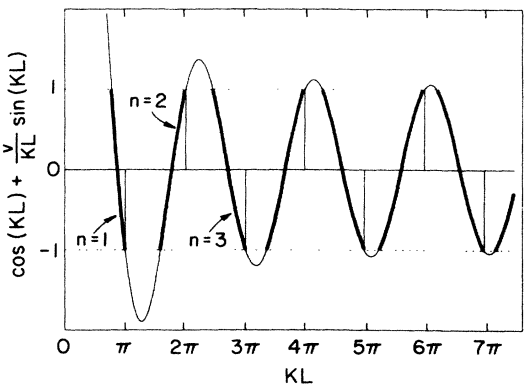

FIG. 25. Graph to determine the allowed and forbidden adiabatic eigenenergies $\varepsilon_{n,\alpha}=\hbar^2K_{n,\alpha}^2/2m$ for the Kronig-Penney model. The heavy lines mark the positions of allowed values for $K_{n,\alpha}L=KL$. The upper edges of the bands are given by $KL=n\pi$, $n=1,2,\ldots$.

APPENDIX B

In this appendix we briefly illustrate how Zener tunneling and backscattering can be cast into the form of a normal scattering problem. As many of the results are spread over the literature and derived in a different way, we give a self-contained derivation here. The time evolution of the coefficients $c_n(\alpha)$ is determined by the system of differential equations (6). This system is simplified by (i) a unitary transformation to the variables

$$b_n(\alpha)=\exp\left[(i/eFL)\int_0^\alpha d\alpha'\varepsilon_{n,\alpha'}\right]c_n(\alpha),$$

and (ii) a choice of phase $-P(\alpha)$ for the eigenfunctions $u_{n,\alpha}(x)$ such that the diagonal matrix elements A_{nn} vanish. As A_{nn} is purely imaginary (due to the normalization of $u_{n,\alpha}$ which does not depend on α) the condition $\mathrm{Im}A_{nn}=0$ can always be satisfied by a suitable choice of $P(\alpha)$. A rather lengthy calculation leads to the result $P(\alpha)=\alpha/2$. Using Eqs. (A6), (3), and the result for $P(\alpha)$ the eigenfunctions $u_{n,\alpha}(x)$ become

$$u_{n,\alpha}=N_{n,\alpha}i^{(n-1)}e^{-i(\alpha/2)}e^{-i\alpha(x/L)}\times(e^{i\mathcal{K}_{n,\alpha}[x+(L/2)]}-q_{n,\alpha}e^{-i\mathcal{K}_{n,\alpha}[x+(L/2)]}). \quad \text{(B1)}$$

Note that whereas $\varphi_{n,-\pi}=\varphi_{n,\pi}^*=\varphi_{n,\pi}$ we find that $u_{n,-\pi}=u_{n,\pi}^*=-\exp(2\pi ix/L)u_{n,\pi}$, i.e., the functions $\varphi_{n,\alpha}$ show the usual symmetries of Bloch functions, whereas the $u_{n,\alpha}$ do not.

Using the results of (i) and (ii) above, the time evolution of the coefficients $b_n(\alpha)$ becomes

$$i\frac{db_n(\alpha)}{d\alpha}=-i\sum_{m\,(\neq n)}A_{nm}(\alpha)\exp\left[(i/eFL)\times\int_0^\alpha d\alpha'(\varepsilon_{n,\alpha'}-\varepsilon_{m,\alpha'})\right]b_m(\alpha). \quad \text{(B2)}$$

Using the relations[27]

$$(u_{n,\alpha},\partial u_{m,\alpha}/\partial\alpha)=\frac{1}{\varepsilon_{m,\alpha}-\varepsilon_{n,\alpha}}(u_{n,\alpha},[\partial H(\alpha)/\partial\alpha]u_{m,\alpha}),$$

we can express the matrix elements A_{nm} by the simpler expressions $D_{nm}(\alpha)\equiv L(u_{n,\alpha},\partial_x u_{m,\alpha})$. We calculate the matrix elements $D_{nm}(\alpha)$ using the expression (B1) for the wave functions $u_{n,\alpha}$, taking advantage also of the orthogonality $(u_{n,\alpha},u_{m,\alpha})=\delta_{nm}$, as well as the periodicity $(u_{n,\alpha}^*u_{m,\alpha})(0)-(u_{n,\alpha}^*u_{m,\alpha})(L)=0$ of the wave functions. The result is

$$D_{nm}(\alpha)=4Li^{(m-n+1)}N_{n,\alpha}N_{m,\alpha}\frac{\mathcal{K}_{n,\alpha}\mathcal{K}_{m,\alpha}}{\mathcal{K}_{m,\alpha}^2-\mathcal{K}_{n,\alpha}^2}(1-q_{n,\alpha}q_{m,\alpha})$$

$$\times\sin(\mathcal{K}_{m,\alpha}-\mathcal{K}_{n,\alpha})\frac{L}{2}\ , \tag{B3}$$

$$D_{nm}(-\alpha)=(-1)^{m+n-1}D_{nm}(\alpha)=D_{nm}^*(\alpha)\ ,$$

$$D_{mn}(\alpha)=-D_{nm}^*(\alpha)\ .$$

So far, all the formalism in Appendixes A and B is exact.

We have studied the dependence of the matrix elements A_{nm} in (B2) on α and on the level pairing n and m. It turns out that (i) neighboring levels couple strongly as they approach each other, and (ii) levels further apart couple only weakly, even- (odd-) numbered pairs of levels do not couple at $\alpha=l\pi$.

In principle the set of Eqs. (B2) can be solved numerically taking into account the coupling to the k nearest neighbors. Here we adopt the following approximations: (i) only the coupling to the nearest approaching level is taken into account, and (ii) we assume the scattering potential $V(x)$ to be weak or the energy $\varepsilon_{n,\alpha}$ of the electron in state n to be large. The approximation (ii) allows us to solve Eq. (A5) perturbatively and we find the results (to leading order in Δ/E_n)

$$LK_{n,\alpha}=n\pi\left[1-\frac{\Delta}{2E_n}\left\{1-\left[1+\left[\frac{w_n}{\pi\Delta}\right]^2\alpha^2\right]^{1/2}\right\}\right] \tag{B3a}$$

for the upper edge of the nth band, and

$$LK_{n+1,\alpha}=n\pi\left[1+\frac{\Delta}{2E_n}\left\{1+\left[1+\left[\frac{w_n}{\pi\Delta}\right]^2\alpha^2\right]^{1/2}\right\}\right] \tag{B3b}$$

for the lower edge of the $n+1$st band ($w_n=2E_1 n$). Here we have chosen the origin $\alpha=0$ to coincide with the closest approach of the two bands and we have introduced the gap parameter $\Delta=V_0/L$. The energy difference between approaching bands then is

$$\varepsilon_{n+1,\alpha}-\varepsilon_{n,\alpha}=2\Delta\left[1+\left[\frac{w_n}{\pi\Delta}\right]^2\alpha^2\right]^{1/2}\ . \tag{B4}$$

We note that, as expected, the gaps $\varepsilon_{n+1,0}-\varepsilon_{n,0}=2\Delta$ approach a constant value for the Kronig-Penney model. Using the approximations (B3) and (B4) we find for the matrix elements $A_{nn+1}(\alpha)$

$$A_{nn+1}(\alpha)=A_{n+1n}(\alpha)=\frac{i\hbar^2}{mL^2}\frac{D_{nn+1}(\alpha)}{\varepsilon_{n,\alpha}-\varepsilon_{n+1,\alpha}}$$

$$=\frac{1}{2i}\frac{w_n}{\pi\Delta}\frac{1}{1+\left[\frac{w_n}{\pi\Delta}\right]^2\alpha^2}\ . \tag{B5}$$

Changing variables to $z=w_n\alpha/\pi\Delta$ we finally obtain the set of equations

$$i\frac{db_{n+1}(z)}{dz}=-\frac{1}{2}\frac{1}{1+z^2}\exp\left[i\gamma_n\int_0^z dy(1+y^2)\right]b_n(z)\ ,$$

$$i\frac{db_n(z)}{dz}=-\frac{1}{2}\frac{1}{1+z^2}\exp\left[-i\gamma_n\int_0^z dy(1+y^2)\right]b_{n+1}(z)\ , \tag{B6}$$

with

$$\gamma_n=\pi\frac{2\Delta}{w_n}\frac{\Delta}{eFL}\ .$$

Equations (B6) have been found before by Lenstra and van Haeringen using a different approach (their result slightly differs from ours due to the use of a different phase in the definition of the coefficients b_n) and were integrated analytically by Eilenberger[20] in the weak field limit $\gamma_n\to\infty$. The strong field limit $\gamma_n\to 0$ has been treated by Sauter and Weisse[28] and by Eilenberger. Starting with a particle in the lower band $b_n(-\infty)=1$, $b_{n+1}(-\infty)=0$, a transition probability

$$t_n^2=e^{-(\pi/2)\gamma n} \tag{B7}$$

is found in both cases of weak and strong field as $z\to\infty$. The regime of intermediate fields strengths has been thoroughly studied by Lenstra and van Haeringen[18] by numerical integration of Eqs. (B6). We have integrated (B6) using a standard Runge-Kutta routine with adaptive stepsize control[29] and we illustrate the result in Fig. 26 for six different values of γ_n. The amplitude b_n starts out at 1 and reaches an asymptotic value in the first quadrant of the complex plane as $z\to\infty$, $b_n(\infty)=r_n\exp(i\chi_n)$ with

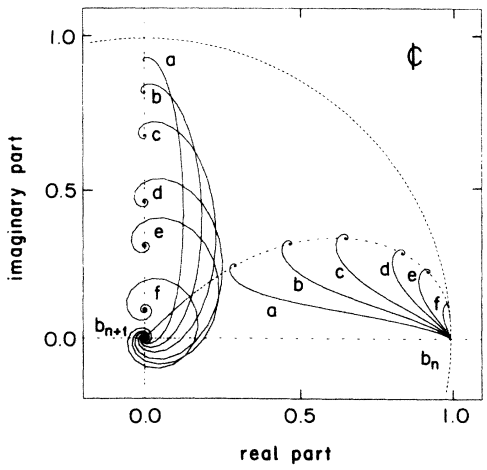

FIG. 26. Time evolution of the amplitudes $b_n(\alpha)$ and $b_{n+1}(\alpha)$ during Zener tunneling between two approaching energy levels. The six pairs of trajectories apply to different values of the electric field F. With $\gamma_n=2\pi\Delta^2/w_n eFL$ we show examples for (a) $\gamma_n=0.1$, a strong field, (b) $\gamma_n=0.25$, (c) $\gamma_n=0.5$, (d) $\gamma_n=1.0$, (e) $\gamma_n=1.5$, and (f) $\gamma_n=3.0$, a weak field. We start with a particle in the lower band, $b_n(-\infty)=1$, $b_{n+1}(-\infty)=0$ and follow the time evolution of the amplitudes as $\alpha\to\infty$. The amplitude for the lower band reaches its asymptotic value in the first quadrant, $b_n(\infty)=r_n e^{i\chi_n}$, the amplitude for the upper band ends up on the imaginary axis due to the time reversal symmetry, $b_{n+1}(\infty)=it_n$.

$0 \le \chi_n \le \pi/4$ and $r_n^2 = 1 - t_n^2$. The amplitude b_{n+1} starts at 0 and ends up on the imaginary axis as $z \to \infty$, $b_{n+1}(\infty) = it_n$. The unitary matrix s_n which relates the initial amplitudes at $z \to -\infty$ to the final amplitudes at $z \to \infty$ then is

$$s_n = \begin{pmatrix} r_n e^{-i\chi_n} & it_n \\ it_n & r_n e^{i\chi_n} \end{pmatrix} . \tag{B8}$$

Note that (B6) has the same symmetry properties as the original Hamiltonian (1) and therefore s_n is unitary and symmetric. In agreement with Lenstra and van Haeringen's observation, we find that Eq. (B7) holds for all field strengths F. We also find the same dependence of χ_n on F as reported in their paper.

In our original problem of Zener tunneling between minibands the integration parameter α runs from $-\pi/2$ to $\pi/2$, therefore we should integrate z in (B6) from $-w_n/2\Delta$ to $w_n/2\Delta$. For the case of a weak potential $V(x)$ and/or high energies $\varepsilon_{n,\alpha}$ the ratio between the bandwidth w_n and the gap 2Δ is always large and we actually reach the asymptotic regions. For the case of low energies $\varepsilon_{n,\alpha}$ (at the bottom of the spectrum) the transition rates t_n and scattering phases χ_n are modified, but we do not expect these minor modifications to have a severe effect on our results. Therefore we extrapolate Eq. (B8) to describe scattering at low energies, too.

A second source of error are the approximations (B4) and (B5) used for the energy difference $\varepsilon_{n+1,\alpha} - \varepsilon_{n,\alpha}$ and the matrix elements $A_{nn+1}(\alpha)$. Again we find very good agreement between these approximations and the exact results (the error in the matrix elements is less than 4% over the entire range $-\pi/2 \le \alpha \le \pi/2$ for $w_n/\Delta = 2$). Note that when generalizing (B7) to smooth scattering potentials $V(x)$ the gap parameter Δ depends on level index n.

Finally transforming back to the coefficients $c_n(\alpha)$ we obtain the scattering matrix S_n

$$S_n = \begin{pmatrix} r_n e^{-i(\chi_n + \Theta_n + \vartheta_n)} & it_n e^{-i\Theta_n} \\ it_n e^{-i\Theta_n} & r_n e^{i(\chi_n - \Theta_n + \vartheta_n)} \end{pmatrix} ,$$

with

$$\Theta_n = \frac{1}{eFL} \int_0^{\pi/2} d\alpha (\varepsilon_{n+1,\alpha} + \varepsilon_{n,\alpha}) ,$$

$$\vartheta_n = \frac{1}{eFL} \int_0^{\pi/2} d\alpha (\varepsilon_{n+1,\alpha} - \varepsilon_{n,\alpha}) .$$

Finally using $\varepsilon_{n+1,\alpha} + \varepsilon_{n,\alpha} = 2(\Delta_n + E_n)$ and (B4) for the difference $\varepsilon_{n+1,\alpha} - \varepsilon_{n,\alpha}$ we have derived Eq. (7).

We finish this appendix with a brief derivation of the current $j(t)$. Using the definition (5) we find

$$j(t) = \frac{e}{\hbar} \sum_n |c_n(t)|^2 \frac{d\varepsilon_{n,\alpha}}{d\alpha} + \frac{e\hbar}{imL^2} \sum_{m \ne n} c_m^*(t) c_n(t) D_{mn}(\alpha) . \tag{B9}$$

The examination of this expression at our sampling points α_{2k} shows that the diagonal term is completely dominating the current carried by the off-diagonal part. We therefore neglect the second term in (B9). Evaluation of $\partial_\alpha \varepsilon_{n,\alpha}$ at the sampling points α_{2k} finally leads to

$$j^{(k)} = j_0 \sum_{n=1}^{\infty} |c_n^{(k)}|^2 (-1)^{n-1} (n - \tfrac{1}{2}) ,$$

with

$$j_0 = \frac{e\hbar\pi}{mL^2} .$$

---

*Permanent address: Asea Brown Boveri, Corporate Research, CH-5405 Baden, Switzerland.

†Present address: Department of Physics and Astronomy, Louisiana State University, Baton Rouge, LA 70803-4001.

[1]For a recent review, see Y. Imry, in *Directions in Condensed Matter Physics: Memorial Volume in Honor of Shang-keng Ma*, edited by G. Grinstein and G. Mazenko (World Scientific, Singapore, 1986).

[2]A. Benoit, C. P. Umbach, R. B. Laibowitz, and R. A. Webb, Phys. Rev. Lett. **58**, 2343 (1987).

[3]W. J. Skocpol, P. M. Mankievich, R. E. Howard, L. D. Jackel, D. M. Tennant, and A. Douglas Stone, Phys. Rev. Lett. **58**, 2347 (1987).

[4]Sean Washburn and Richard A. Webb, Adv. Phys. **35**, 375 (1986).

[5]G. Timp, A. Chang, P. Mankiewich, T. Y. Chang, R. Behringer, J. E. Cunningham, and R. Howard, Phys. Rev. Lett. **59**, 732 (1987).

[6]M. Büttiker, Y. Imry, and R. Landauer, Phys. Lett. **96A**, 365 (1983).

[7]M. Büttiker, Y. Imry, and M. Ya. Azbel, Phys. Rev. A **30**, 1982 (1984).

[8]R. Landauer and M. Büttiker, Phys. Rev. Lett. **54**, 2049 (1985).

[9]M. Büttiker, Y. Imry, R. Landauer, and S. Pinhas, Phys. Rev. B **31**, 6207 (1985).

[10]C. Zener, Proc. R. Soc. London, Ser. A **137**, 696 (1932); *ibid.* **A145**, 523 (1934).

[11]D. Lenstra and W. van Haeringen, Phys. Rev. Lett. **57**, 1623 (1986).

[12]D. Lenstra and W. van Haeringen, J. Phys. C **14**, 5293 (1981).

[13]D. Lenstra and W. van Haeringen, J. Phys. C **14**, L819 (1981).

[14]D. Lenstra and W. van Haeringen, Physica B + C **128B**, 26 (1985).

[15]R. Landauer, Phys. Rev. Lett. **58**, 2150 (1987), comment on Ref. 11.

[16]D. Lenstra and W. van Haeringen, Phys. Rev. Lett. **58**, 2151 (1987), reply to Ref. 15.

[17]R. Landauer, Phys. Rev. B **33**, 6497 (1986).

[18]D. Lenstra, H. Ottevanger, W. van Haeringen, and A. G. Tijhuis, Phys. Scr. **34**, 438 (1986).

[19]N. Byers and C. N. Yang, Phys. Rev. Lett. **7**, 46 (1961).

[20]G. Eilenberger, Z. Phys. **164**, 59 (1961).

[21]S. Fishman, D. R. Grempel, and R. E. Prange, Phys. Rev. Lett. **49**, 509 (1982); D. R. Grempel, R. E. Prange, and Shmu-

el Fishman, Phys. Rev. A **29**, 1639 (1984).
[22]Ping Ao (private communication).
[23]M. Abramowitz and I. A. Stegun, *Handbook of Mathematical Functions* (Dover, New York, 1972).
[24]N. G. van Kampen, *Stochastic Processes in Physics and Chemistry* (North-Holland, Amsterdam, 1981).
[25]John H. Davies (unpublished).
[26]D. S. Saxon and R. A. Hutner, Philips Res. Rep. **4**, 81 (1949).
[27]A. B. Migdal and V. P. Krainov, *Approximation Methods in Quantum Mechanics* (Benjamin, New York, 1969), p. 83.
[28]F. Sauter and J. Weisse, Z. Phys. **140**, 150 (1955).
[29]W. H. Press, B. P. Flannery, S. A. Teukolsky, and W. T. Vetterling, *Numerical Recipes* (Cambridge University Press, Cambridge, 1986).

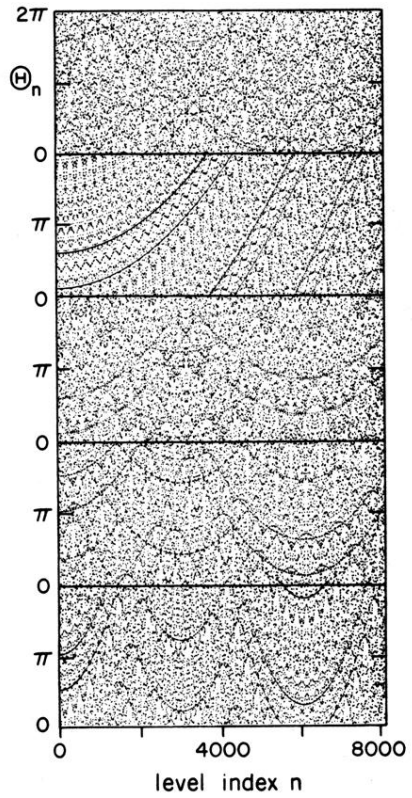

FIG. 10. Phase map Θ_n as a function of level index n for five different values of the electric field F; from top to bottom $F=9$, 7, 5, 3, and 1, respectively. Since the phase parameter $\tau=E_1/eFL$ depends on the field, the phase maps change with field. Quasiperiods appear when τ is well approximated by a rational μ/ν; the length of the quasiperiod is given by ν. Again the behavior of the phases Θ_n is essentially random on short scales.

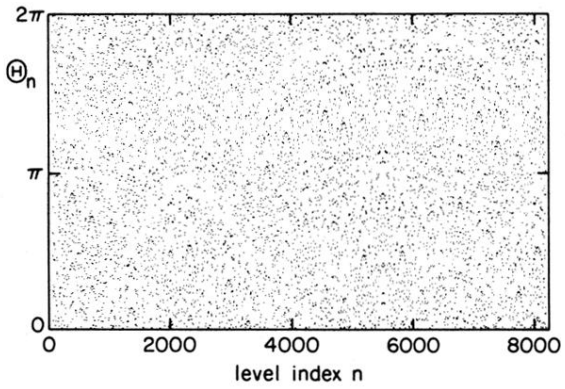

FIG. 4. Phase Θ_n picked up during a single forward scattering event as a function of level index n. The phase parameter $\tau = E_1/eFL$ has been chosen equal to the inverse of the golden mean $\tau_G = (1+\sqrt{5})/2$, $\tau = 1/\tau_G$. The phases Θ_n are found by taking the modulus of $\pi\tau n^2$ with respect to 2π. The quasiperiodic patterns which appear on a large scale in n are due to close approximations of τ by a rational μ/ν, generating quasiperiods of length ν. Most important, however, is the locally random behavior of the phases Θ_n.